Master of Science Thesis in Electrical Engineering
Department of Electrical Engineering, Linköping University, 2021

Linearization Based Model Predictive Control of a Diesel Engine with Exhaust Gas Recirculation and Variable-Geometry Turbocharger

Jonatan Gustafsson

LINKÖPING UNIVERSITY

Master of Science Thesis in Electrical Engineering

Linearization Based Model Predictive Control of a Diesel Engine with Exhaust Gas Recirculation and Variable-Geometry Turbocharger

Jonatan Gustafsson

LiTH-ISY-EX–21/5363–SE

Supervisor: **Viktor Leek**
ISY, Linköping University

Examiner: **Jan Åslund**
ISY, Linköping University

Division of Vehicular Systems
Department of Electrical Engineering
Linköping University
SE-581 83 Linköping, Sweden

Copyright © 2021 Jonatan Gustafsson

Abstract

Engine control systems aim to ensure satisfactory output performance whilst adhering to requirements on emissions, drivability and fuel efficiency. Model predictive control (MPC) has shown promising results when applied to multivariable and nonlinear systems with operational constraints, such as diesel engines. This report studies the torque generation from a mean-value heavy duty diesel engine with exhaust gas recirculation and variable-geometry turbocharger using state feedback linearization based MPC (LMPC). This is accomplished by first introducing a fuel optimal reference generator that converts demands on torque and engine speed to references on states and control signals for the MPC controller to follow. Three different MPC controllers are considered: a single linearization point LMPC controller and two different successive LMPC (SLMPC) controllers, where the controllers are implemented using the optimization tool CasADi. The MPC controllers are evaluated with the World Harmonized Transient Cycle and the results show promising torque tracking using a SLMPC controller with linearization about reference values.

Acknowledgments

I would first like to thank my supervisor, Viktor Leek, whose feedback has helped me immensely. Viktor has kindly answered all my questions and his expertise has been invaluable.

I would also like to thank my examiner Jan Åslund who has scrutinized and supported the project from idea to execution.

In addition, I would like to acknowledge my opponent Joakim Säfdal for proofreading my report.

And finally, I would like to thank my family and friends. You have made my academical journey possible.

Thank you!

Järfälla, February 2021
Jonatan Gustafsson

Contents

List of Figures x

List of Tables xii

Notation xiii

1 Introduction 1
- 1.1 Motivation . . . 1
- 1.2 Aim . . . 2
- 1.3 Problem Formulation . . . 2
- 1.4 Delimitations . . . 3

2 Theory 5
- 2.1 Control Aspects of Diesel Engines . . . 5
- 2.2 Numerical Optimal Control . . . 6
  - 2.2.1 Convex and Nonconvex Optimization . . . 6
  - 2.2.2 Direct Methods . . . 6
  - 2.2.3 Numerical Integration Methods . . . 7
- 2.3 CasADi . . . 8
- 2.4 Model Predictive Control . . . 9
  - 2.4.1 Design Concepts . . . 9
  - 2.4.2 Linearization Based MPC . . . 11
  - 2.4.3 Successive Linearization Based MPC . . . 12
- 2.5 Evaluation of Controller Performance . . . 12
- 2.6 World Harmonized Transient Cycle . . . 13

3 System Overview 15
- 3.1 Model . . . 15
  - 3.1.1 Model Delimitation . . . 16
  - 3.1.2 Model Summary . . . 16
  - 3.1.3 Control Challenges . . . 20
- 3.2 Reference Generator . . . 20
- 3.3 Model Predictive Controller . . . 21

4 Reference Generator **23**
4.1 Engine Map Methodology . . . 23
4.1.1 Relaxed Optimization Problem . . . 24
4.1.2 Design Parameters . . . 24
4.1.3 Engine Map . . . 25
4.2 Lookup Tables . . . 26
4.2.1 Negative Torque Inputs . . . 26
4.2.2 Relaxed Solutions . . . 27

5 Model Predictive Control **29**
5.1 Control Designs . . . 29
5.1.1 Linearization Based MPC . . . 30
5.1.2 Successive Linearization Based MPC . . . 31
5.2 Measurements of Controller Performance . . . 31
5.2.1 Tracking Error . . . 32
5.2.2 Fuel Consumption . . . 32
5.2.3 Mechanical Work . . . 32

6 Results **33**
6.1 Controller Design . . . 34
6.1.1 Design Parameters . . . 34
6.1.2 Time Horizon using Preview . . . 34
6.1.3 Integral Action . . . 34
6.2 Linearization Based MPC . . . 35
6.2.1 Transient Response . . . 35
6.2.2 Ramp Response . . . 37
6.2.3 Sinusoidal Response . . . 38
6.2.4 Drawback . . . 38
6.3 Successive Linearization Based MPC about Current Operating Point 39
6.3.1 Transient Response . . . 39
6.3.2 Ramp Response . . . 41
6.3.3 Sinusoidal Response . . . 42
6.4 Successive Linearization Based MPC about Reference Values . . . 42
6.4.1 Transient Response . . . 42
6.4.2 Ramp Response . . . 44
6.4.3 Sinusoidal Response . . . 45
6.5 Evaluation of Controller Performance . . . 45

7 Discussion and Conclusions **49**
7.1 Design Concepts . . . 49
7.1.1 Weight Matrices . . . 49
7.1.2 Sampling Rate . . . 49
7.1.3 Time Horizon . . . 50
7.1.4 Preview . . . 50
7.1.5 Integral Action . . . 50
7.2 Controller Performance . . . 50

7.2.1 Smoke Limiter 51
7.3 Future Work 51
7.4 Conclusions 52

A MATLAB Model Representation **55**
A.1 MATLAB Model 55
A.2 MATLAB Model Validation 55

B De-Normalization of WHTC **59**
B.1 Speed Profile 59
B.2 Torque Profile 60
B.3 De-Normalized Test Data 61

C Lookup Table Data **63**
C.1 State Reference Values 63
C.2 Control Signal Reference Values 65

D Weight Matrices **67**

Bibliography **69**

List of Figures

1.1 Sketch of the problem 2

2.1 World Harmonized Transient Cycle 13

3.1 Overview of system including reference generator, MPC controller and system model 15
3.2 Model structure of the diesel engine. Reprinted with permission from Wahlström and Eriksson [24] 16
3.3 Illustration of non-minimum phase behaviors from u_{egr} to p_{im} (left), and u_{vgt} to W_{c} (right) 20
3.4 Overview of reference generator 21
3.5 Overview of linearization based MPC controller 21

4.1 Engine map: solutions to (4.1) and (4.2) 25
4.2 Illustration of table data (left) and its derivative (right) 26
4.3 Inputs and outputs to the lookup tables 26
4.4 Simulation of 0% torque at 500 rpm: states and control signals . . 27
4.5 Simulation of 0% torque at 500 rpm: engine torque 27

6.1 Effect of time horizon using LMPC with preview: transient from 650 Nm to 2000 Nm at 1200 rpm 34
6.2 Effect of integral action using SLMPC about current operating point: transient from 800 Nm to 2000 Nm at 1200 rpm 35
6.3 Transient from 800 Nm to 900 Nm at 1200 rpm: LMPC 36
6.4 Transient from 650 Nm to 2000 Nm at 1200 rpm: LMPC 36
6.5 Ramp response at 1200 rpm: LMPC 37
6.6 Sinusoidal response at 1200 rpm: LMPC 38
6.7 Transient from 650 Nm to 2000 Nm at 700 rpm: LMPC 39
6.8 Transient from 800 Nm to 900 Nm at 1200 rpm: SLMPC about current operating point 40
6.9 Transient from 650 Nm to 2000 Nm at 1200 rpm: SLMPC about current operating point 40
6.10 Ramp response at 1200 rpm: SLMPC about current operating point 41
6.11 Sinusoidal response at 1200 rpm: SLMPC about current operating point 42

6.12 Transient from 800 Nm to 900 Nm at 1200 rpm: SLMPC about reference values . . . 43
6.13 Transient from 650 Nm to 2000 Nm at 1200 rpm: SLMPC about reference values . . . 43
6.14 Ramp response at 1200 rpm: SLMPC about reference values . . . 44
6.15 Sinusoidal response at 1200 rpm: SLMPC about reference values . 45
6.16 WHTC torque tracking comparison between LMPC and SLMPC using integral action. Negative torque values can be ignored (closed rack motoring) . . . 46
6.17 Zoom of Figure 6.16 from 1290 to 1460 s . . . 47

A.1 State comparison between MATLAB model and Simulink model . 56
A.2 Engine torque and oxygen-to-fuel ratio comparison between MATLAB model and Simulink model . . . 56
A.3 Absolute errors normalized with respect to state means for comparison in Figure A.1 . . . 57

B.1 Maximum torque curve, $M_{\max/n}$, for stationary points . . . 61
B.2 De-normalized test data. . . . 62

C.1 Lookup table data for intake manifold pressure, p_{im}, and its derivative, $\frac{d}{dt}p_{\text{im}}$ . . . 63
C.2 Lookup table data for exhaust manifold pressure, p_{em}, and its derivative, $\frac{d}{dt}p_{\text{em}}$ . . . 64
C.3 Lookup table data for intake manifold oxygen mass fraction, X_{Oim}, and its derivative, $\frac{d}{dt}X_{\text{Oim}}$ . . . 64
C.4 Lookup table data for exhaust manifold oxygen mass fraction, X_{Oem}, and its derivative, $\frac{d}{dt}X_{\text{Oem}}$ . . . 64
C.5 Lookup table data for turbine speed, ω_{t}, and its derivative, $\frac{d}{dt}\omega_{\text{t}}$. 65
C.6 Lookup table data for injected fuel per cylinder, u_δ . . . 65
C.7 Lookup table data for EGR control signal, u_{egr} . . . 66
C.8 Lookup table data for VGT control signal, u_{vgt} . . . 66

List of Tables

3.1 Description of states 17
3.2 Description of control signals 17
3.3 Description of parameters and variables 18

6.1 Controller performance data where IA and P denote integral action and preview respectively 46

B.1 Rescaled engine speeds used for de-normalization. 60

Notation

Acronyms

Notation	Description
MPC	Model Predictive Control
LMPC	Linearization Based MPC
SLMPC	Successive Linearization Based MPC
EGR	Exhaust Gas Recirculation
VGT	Variable-Geometry Turbocharger
ICE	Internal Combustion Engine
WHTC	World Harmonized Transient Cycle
PID	Proportional, Integral, Differential (controller)

Symbols

Notation	Description	Unit
c_{fric}	Friction coefficient	-
e	Tracking/reference error	-
E_{m}	Mechanical work	J
h	Step size	s
J_{t}	Turbine moment of inertia	$\text{kg} \cdot \text{m}^2$
m	Mass	kg
M	Torque	$\text{N} \cdot \text{m}$
M_{desired}	Desired/reference torque	$\text{N} \cdot \text{m}$
M_{e}	Engine torque	$\text{N} \cdot \text{m}$
M_{p}	Pumping torque	$\text{N} \cdot \text{m}$
n_{cyl}	Number of cylinders	-
n_{e}	Rotational engine speed	rpm
N	Prediction horizon	-
$(\text{O/F})_{\text{s}}$	Stoichiometric oxygen-to-fuel ratio	-
p	Pressure	Pa
P	Power	W
q_{HV}	Heating value of fuel	J/kg
Q	Weight matrix	-
r	Reference vector	-
$\boldsymbol{r}$	Reference vector sequence	-
R	Gas constant	$\text{J}/(\text{kg} \cdot \text{K})$
T	Time horizon	s
T_{cycle}	Test cycle time	s
T_{im}	Intake manifold temperature	K
T_{em}	Exhaust manifold temperature	K
T_{s}	Sampling rate	s
u	Control signal vector	-
$\boldsymbol{u}$	Control signal vector sequence	-
u_{egr}	EGR control signal	%
u_{vgt}	VGT control signal	%
u_{δ}	Injected amount of fuel	mg/cycle
V	Volume	m^3
W	Mass flow	kg/s
x	State vector	-
$\boldsymbol{x}$	State vector sequence	-
x_0	State initial condition	-
x_{egr}	EGR-fraction	-
y	Output vector	-
X_{O}	Oxygen mass fraction	-
η	Efficiency	-
λ	Air-to-fuel ratio	-
λ_{O}	Oxygen-to-fuel ratio	-
ω	Rotational speed	rad/s

Subscripts

Notation	Description
a	Air
c	Compressor
c	Continuous time
d	Displaced
e	Engine
egr	EGR
ei	Engine cylinder in
em	Exhaust manifold
eo	Engine cylinder out
f	Fuel
f	Final/Terminal
fric	Friction
ig	Indicated gross
im	Intake manifold
m	Mechanical
ref	Reference value
t	Turbine
vgt	VGT
δ	Fuel injection

1 Introduction

This thesis focuses on linearization based model predictive control (MPC) of a heavy duty diesel engine with exhaust gas recirculation (EGR) and variable-geometry turbocharger (VGT). The following sections introduce the problem of interest.

1.1 Motivation

Diesel engines must meet increasingly stricter emission requirements while also satisfying requirements on drivability and fuel efficiency. Control systems aim to ensure satisfactory output performance whilst adhering to the requirements and input constraints. Model predictive control has shown promising results when applied to multivariable and nonlinear systems with operational constraints, such as diesel engines [21].

Model-based control techniques, such as MPC, take advantage of models – which entails that more time can be used to calibrate models instead of calibrating traditional controllers. This is especially advantageous when working with physics-based models, that is where the model correctly represents the input-output relationship, as it results in greater understanding of the control process.

Heavy duty diesel engines with EGR and VGT have tricky system control properties such as non-minimum phase behaviours, overshoot, sign reversal and coupling [24]. A mean-value model of the heavy duty diesel engine is used to investigate and evaluate linearization based MPC design using the World Harmonized Transient Cycle (WHTC) as test cycle. The model facilitates swift and cheap testing as MPC can be implemented in MATLAB and Simulink using the optimization tool CasADi.

1.2 Aim

This master thesis will focus on torque generation from a heavy duty diesel engine with EGR and VGT using linearization based MPC. The aim is to minimize fuel consumption through the added fuel power P_f. The minimization should still provide the required engine torque, M_e, given a known engine rotational speed, n_e, and desired torque, $M_{desired}$, as shown in Figure 1.1.

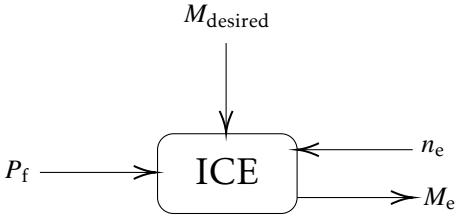

Figure 1.1: *Sketch of the problem*

In other words the desired mechanical power P_m should ideally follow (1.1).

$$P_m = M_e \omega_e = \frac{30}{\pi} M_e n_e = \frac{30}{\pi} M_{desired} n_e \tag{1.1}$$

Furthermore, the thesis aims to evaluate and compare performances of linearization based MPC designs for the heavy duty internal combustion engine (ICE).

1.3 Problem Formulation

This master thesis aims to answer the following questions:

- How can linearization based MPC be applied to control the fuel and air path of the diesel engine?
- How can performance requirements, such as torque response time, and requirements on safe operation, such as turbocharger overspeed protection, be introduced in the MPC controller?
- How can diesel engine controller performances be measured and compared?
- How do the considered linearization based MPC controllers compare in terms of performance?

1.4 Delimitations

The delimitations for this thesis are:

- The controllers proposed in this report are evaluated on a validated model of a diesel engine with EGR and VGT [24]. The model delimitations are presented in Section 3.1.1.
- Computational time and memory are neglected when comparing controller performances.
- The test speeds for the de-normalization of the speed profile in WHTC are approximated using test speeds from a hybrid electric truck engine, see Chapter B. This results in somewhat realistic speed values that suffice for examining torque generation, but not good enough to run emission tests.
- Ethical and societal aspects related to the work are not considered.

2

Theory

Related research for this thesis focuses on six main fields: control aspects of diesel engines, CasADi, numerical optimal control, model predictive control, measurement of controller performance and the World Harmonized Transient Cycle. Each field is presented in the sections below.

2.1 Control Aspects of Diesel Engines

Diesel engines are the most efficient internal combustion engines with two major drawbacks: low power density and problematic exhaust gas purification. The former is eliminated by the use of turbochargers as the turbocharger forces more air into the cylinders which allows more fuel to be burned in the same volume. EGR partly accounts for the latter drawback as the recirculation of exhaust gas leads to less oxygen in the combustion process as well as a lowered combustion temperature. Thus, an increased intake manifold EGR-fraction, x_{egr}, results in a reduced amount of unwanted in-cylinder nitric oxide formation, NO_x. Additionally, particulate matter can be reduced by increasing the oxygen-to-fuel ratio, λ_O. However, control designs become highly complex when introducing EGR and turbochargers, such as VGT.[11, 24]

The main control objectives for heavy duty diesel engines are [13]:

- Fast reference tracking of torque
- Minimal fuel consumption
- Low emissions of NO_x
- Low emissions of smoke

- Limited emission peaks during transients
- Limited peak pressure derivatives to avoid audible noise and engine damage

2.2 Numerical Optimal Control

Numerical optimal control methods are at the core of every MPC implementation [19]. In consequence the algorithmic choices heavily affect the performance and reliability of the controllers. Continuous and discrete time MPC optimization problems have the structure presented in (2.1) and (2.2) respectively.

$$\begin{aligned} \min_{x(\cdot),u(\cdot)} \quad & \int_0^T \ell_c(x(t),u(t))dt + V_f(x(T)) \\ \text{subject to} \quad & x(0) = x_0 \\ & \dot{x}(t) = f_c(x(t),u(t)), \quad t \in [0,T] \\ & h(x(t),u(t)) \leq 0, \quad t \in [0,T] \\ & h_f(x(T)) \leq 0 \end{aligned} \tag{2.1}$$

$$\begin{aligned} \min_{\boldsymbol{x},\boldsymbol{u}} \quad & \sum_{k=0}^{N-1} \ell(x(k),u(k)) + V_f(x(N)) \\ \text{subject to} \quad & x(0) = x_0 \\ & x(k+1) = f(x(k),u(k)), \quad k = 0,1,\ldots,N-1 \\ & h(x(k),u(k)) \leq 0, \quad k = 0,1,\ldots,N-1 \\ & h_f(x(N)) \leq 0 \end{aligned} \tag{2.2}$$

where T is the time horizon, N the prediction horizon and x_0 the state initial condition. In the discrete time setting $\boldsymbol{u} = (u(0),u(1),\ldots,u(N-1))$ is the control signal vector sequence and $\boldsymbol{x} = (x(0),x(1),\ldots,x(N))$ the state vector sequence whereas the continuous time setting deals with infinitely large sequences.[19]

2.2.1 Convex and Nonconvex Optimization

An important aspect of optimization is the difference between convex and nonconvex optimization. In brief, convex optimization problems have both convex cost functions and convex constraints whereas nonconvex problems do not. Most importantly, for convex problems every local minimum is also a global minimum whereas nonconvex problems cannot guarantee global minimums or – in worst case – any solution at all.[19]

2.2.2 Direct Methods

There are various methods to numerically solve continuous time optimal control problems on the form (2.1). Direct methods discretize continuous time optimal control problems into finite-dimensional optimization problems, and the meth-

ods are commonly used in MPC applications when working with continuous time system dynamics.[19]

To illustrate the discretization (2.1) is considered. In direct methods the continuous index $t \in [0, T]$ is divided into discrete steps with step size $h = T/N$ and evaluated for the discrete time points $t = hk$. Additionally, the objective integral in (2.1) is replaced with a Riemann sum and the derivative by, for instance, an approximation $\dot{x}(t) \approx \frac{x(t+h)-x(t)}{h}$. The resulting optimal control problem then has the form (2.3).

$$\begin{aligned} \min_{\boldsymbol{x},\boldsymbol{u}} \quad & \textstyle\sum_{t\in\mathbb{H}} h\ell_c(x(t),u(t)) + V_f(x(Nh)) \\ \text{subject to} \quad & x(0) = x_0 \\ & \tfrac{x(t+h)-x(t)}{h} = f_c(x(t),u(t)), \quad t \in \mathbb{H} \\ & h(x(t),u(t)) \leq 0, \quad t \in \mathbb{H} \\ & h_f(x(Nh)) \leq 0 \end{aligned} \tag{2.3}$$

where $\mathbb{H} = \{0, h, 2h, \ldots, (N-1)h\}$, $\boldsymbol{u} = (u(0), u(h), \ldots, u(Nh-h))$ and $\boldsymbol{x} = (x(0), x(h), \ldots, x(Nh))$. The modified formulation (2.3) is comparable to the discrete time formulation (2.2) using $\ell(x,u) = h\ell_c(x,u)$ and $f(x,u) = x + hf_c(x,u)$. The approximation of the differential equation $\dot{x}(t) = f_c(x(t),u(t))$ can, however, be done using any numerical integration method, see Section 2.2.3.[19]

Direct Multiple Shooting

A common direct method is direct multiple shooting. The finite-dimensional optimization problem for direct multiple shooting is formulated as (2.4).

$$\begin{aligned} \min_{\boldsymbol{s},\boldsymbol{q}} \quad & \textstyle\sum_{i=0}^{N-1} \ell_i(s_i,q_i) + V_f(s_N) \\ \text{subject to} \quad & s_0 = x_0 \\ & s_{i+1} = \bar{x}_i(t_{i+1}; s_i, q_i), \text{ for } i = 0,\ldots,N-1 \\ & H_i(s_i,q_i) \leq 0, \text{ for } i = 0,1,\ldots,N-1 \\ & h_f(s_N) \leq 0 \end{aligned} \tag{2.4}$$

where $\boldsymbol{s} = (s_0, s_1, \ldots, s_N)$ are states, $\boldsymbol{q} = (q_0, q_1, \ldots, q_{N-1})$ are the constant control values from piecewise control signal discretization, $\ell_i(s_i,q_i)$ is the numerically approximated continuous objective integral for each interval, and $\bar{x}_i(t; s_i, q_i)$ is the numerical solution to the initial-value problems of the continuous system dynamics for each interval. The multiple shooting formulation (2.4) is then comparable to the discrete time optimal control problem (2.2) and can therefore be solved in discrete time.[19]

2.2.3 Numerical Integration Methods

Numerical simulations of ordinary differential equations $\dot{x} = f(x,u)$ are mostly relevant when solving continuous time optimal control problems. Two common

numerical integration methods are: the forward Euler integrator and the classical 4th order Runge-Kutta integrator.

Forward Euler Integrator

The forward Euler integrator is a first order integrator that offers moderate accuracy. Note that here $\bar{x}$ denotes approximated solutions.

Algorithm 1 Forward Euler integrator

$\bar{x}(t+h) = \bar{x}(t) + hf(t, \bar{x})$

The Classical 4th Order Runge-Kutta

A classical and widely used numerical integrator is the 4th order Runge-Kutta integrator. The method is accurate but also of high order.[19]

Algorithm 2 The classical 4th order Runge-Kutta, RK4

$k_1 = f(t, \bar{x})$
$k_2 = f(t + h/2, \bar{x} + (h/2)k_1)$
$k_3 = f(t + h/2, \bar{x} + (h/2)k_2)$
$k_4 = f(t + h, \bar{x} + hk_3)$
$\bar{x}(t+h) = \bar{x}(t) + (h/6)k_1 + (h/3)k_2 + (h/3)k_3 + (h/6)k_4$

2.3 CasADi

CasADi is an open-source framework for algorithmic differentiation and nonlinear programming. In particular interest are the solver for quadratic programming problems (qpOASES) and the Interior Point Optimizer (IPOPT) that can be used to solve nonlinear programming problems.

Quadratic Programs Quadratic programs are defined by convex quadratic cost functions and linear constraints. Globally optimal solutions can usually be found in polynomial time due to the convexity of the program.[3]

The quadratic solver qpOASES offers hot-start efficiency which has comparatively improved optimization performance when working with repetitive optimization problems that do not differ much after each iteration. The speed-up ranges from 10-30x, and sometimes even up to 80x, faster solving times compared to without hot-start efficiency.[14]

Nonlinear Programs IPOPT expects nonlinear programs on the form (2.5) [3]. Equality constraints can be introduced by setting the upper and lower bounds to equal values.

$$\begin{aligned} \min_{x} \quad & f(x,p) \\ \text{subject to} \quad & x_{\text{lb}} \leq x \leq x_{\text{ub}} \\ & g_{\text{lb}} \leq g(x,p) \leq g_{\text{ub}} \end{aligned} \tag{2.5}$$

2.4 Model Predictive Control

MPC has grown increasingly popular over the decades, especially in the industries. The method is a form of feedback control that calculates the next sequence of control signals by solving an optimal control problem where system models and other limitations are included as constraints. The optimization problem is usually solved for each sample and therefore the method becomes more and more computationally heavy when working with complex systems with short sampling rates.[6]

Unlike regular optimal control, MPC is a type of closed-loop control where the finite optimal control problem is recomputed with periodically updated measures of initial conditions [16]. The optimal control problem has the structure (2.1) or (2.2) depending on if a continuous or discrete time system is studied, and direct methods are useful to discretize the problem for the former (see Section 2.2.2).[19]

However, MPC controller designs always work in discrete time calculations where the MPC algorithm has the following structure [6]:

Algorithm 3 MPC algorithm

1: Measure states $x(k)$
2: Calculate the control signal sequence $\boldsymbol{u}$ by solving an optimal control problem on the form (2.2)
3: Apply the first control signal $u(k)$ from the sequence $\boldsymbol{u}$ during one sample
4: Update time, $k := k + 1$
5: Repeat from step 1

2.4.1 Design Concepts

This section aims to introduce some important concepts for MPC design.

Reference Tracking

Reference tracking is a common concept in control design. In MPC design reference tracking is easily introduced by including the reference in the cost function, as illustrated for a given time k in the example below.

$$\sum_{j=0}^{N-1} \|y(k+j) - r(k+j)\|_{Q_1}^2 + \|u(k+j)\|_{Q_2}^2$$

An advantage with MPC is that the reference can include future reference values, for instance $\boldsymbol{r} = (r(k), r(k+1), \ldots, r(k+N-1))$. This is called *preview*. However, in some cases the future reference is not available and the reference is instead assumed to be constant, $r(k+j) = r(k)$.[6] Control signal reference tracking is implemented similarly [5].

Integral Action

Integral action aims to eliminate stationary control errors. One method to introduce integral action is to penalize increments in the control signals instead of the amplitude, as illustrated in the example below.[6] However, it is easy to add an additional penalty to $u(k+j)$ as well [12].

$$\sum_{j=0}^{N-1} \|y(k+j) - r(k+j)\|_{Q_1}^2 + \|u(k+j) - u(k+j-1)\|_{Q_3}^2$$

Constraints

As mentioned earlier an advantage with MPC is the ability to deal with system requirements such as requirements on states, control signals, overshoot and much more. The requirements are easily included as constraints in the optimization problem.[6]

Output Selection

Output selection is important for the MPC design as it directly affects the optimization problem and the resulting performance of the controller. This section will present common output selections for diesel engines. The most common choice of outputs are compressor mass flow and intake manifold pressure, see (2.6), since the two are combustion related and often directly measurable [4, 25].

$$y = \begin{pmatrix} W_c & p_{im} \end{pmatrix}^\intercal \tag{2.6}$$

Though, there is a problem with this choice of outputs: if a set-point for compressor mass flow or intake manifold pressure is unreachable, tracking of the other reference cannot be guaranteed (even if its set-point is reachable). Consequently, the set-points have to be limited to reachable values to avoid the set-point problem.[18, 25]

Another output choice is EGR-fraction, x_{egr}, oxygen-to-fuel ratio, λ_O, and pumping losses, $p_{em} - p_{im}$, see (2.7).

$$y = (x_{\text{egr}} \quad p_{\text{em}} - p_{\text{im}} \quad \lambda_{\text{O}})^{\intercal} \tag{2.7}$$

With these outputs unreachable set-points are handled. Additionally, the EGR-fraction and oxygen-to-fuel ratio are linked to the emissions and the pumping losses are linked to the fuel consumption. Therefore, emissions and fuel consumption can easily be minimized in the cost function of the optimization problem.

A performance comparison between (2.6) and (2.7) shows that MPC with EGR-fraction, oxygen-to-fuel ratio and pumping losses as outputs result in faster torque response and general improved performance.[25]

Moreover, air/EGR mass flow and intake manifold pressure are chosen as outputs in [20], and torque, NO_x, and smoke emissions in [1].

2.4.2 Linearization Based MPC

Linearization based MPC design is based on local linear models obtained by linearizing nonlinear models about linearization points. Thereafter the MPC design can easily be formulated as a quadratic program with the linearized model as a linear constraint.

Stationary Points

Stationary points are calculated using the system state space form, for instance many nonlinear systems can be written on the form (2.8), which has the stationary point (x^*, u^*) when solving (2.9). Nonlinear systems can have several stationary points.[10]

$$\dot{x} = f(x, u) \tag{2.8}$$

$$f(x^*, u^*) = 0 \tag{2.9}$$

Linearization

A linearization of the system (2.8) about the linearization point (a, b) follows from the Taylor expansion, see (2.10).

$$\begin{aligned} \dot{\tilde{x}} &\approx f(a,b) + \left.\frac{\partial f(x,u)}{\partial x}\right|_{a,b} (x-a) + \left.\frac{\partial f(x,u)}{\partial u}\right|_{a,b} (u-b) \\ &:= A(x-a) + B(u-b) + K = \tilde{f}(x,u) \end{aligned} \tag{2.10}$$

where $\dot{\tilde{x}}$ denotes the linearized system dynamics, and the term $f(a, b) = 0$ if $(a, b) = (x^*, u^*)$ is a stationary point in accordance with (2.9).[10]

2.4.3 Successive Linearization Based MPC

Successive linearization based MPC design is based on the linearization concept in Section 2.4.2. The idea with the controller is to linearize the continuous time nonlinear model at every sampling instant.[26]

2.5 Evaluation of Controller Performance

A controller should provide satisfactory performance and it is therefore important to have a quantifiable measurement of controller performance. Errors in terms of control theory are usually defined as deviation from a certain set-point or reference (denoted $e(t)$ or $e(k)$) during a test response. A few performance measurements for continuous time applications are: Integral Error (IE), Integral Absolute Error (IAE) and Integral Squared Error (ISE), see (2.11).

$$\text{IE} = \int_0^\infty e(t)dt \tag{2.11a}$$

$$\text{IAE} = \int_0^\infty |e(t)|dt \tag{2.11b}$$

$$\text{ISE} = \int_0^\infty [e(t)]^2 dt \tag{2.11c}$$

Naturally, controllers with low cumulative error are desired, but there is a risk of cancellation in IE as the integrand can be both positive and negative. Consequently, IE is not normally used.[15] The measurements are transferable to discrete time systems.

There have been attempts to improve the functionality of (2.11) for diesel control objectives [9, 17, 22]. Furthermore, the error measurements (2.12) have been used to compare PID and MPC controllers for output selection (2.7), that is EGR-fraction, oxygen-to-fuel ratio and pumping losses [25].

$$E_{\lambda_\text{O}} = \sum_{i=1}^{N} \max(\lambda_\text{O}^s(t_i) - \lambda_\text{O}(t_i), 0) \tag{2.12a}$$

$$E_{x_\text{egr}} = \sum_{i=1}^{N} |x_\text{egr}^s(t_i) - x_\text{egr}(t_i)| \tag{2.12b}$$

$$PMEP = \sum_{i=1}^{N} (p_\text{em}(t_i) - p_\text{im}(t_i)) \tag{2.12c}$$

2.6 World Harmonized Transient Cycle

The transient test cycle WHTC is defined in UN Global Technical Regulation No. 4. The cycle includes both cold and hot start requirements, and it is based on world-wide heavy vehicle use. The WHTC consist of a 1800 second-by-second sequence of normalized engine torque and engine speed, see Figure 2.1. Negative torque values are an arbitrary representation of closed rack motoring.[23]

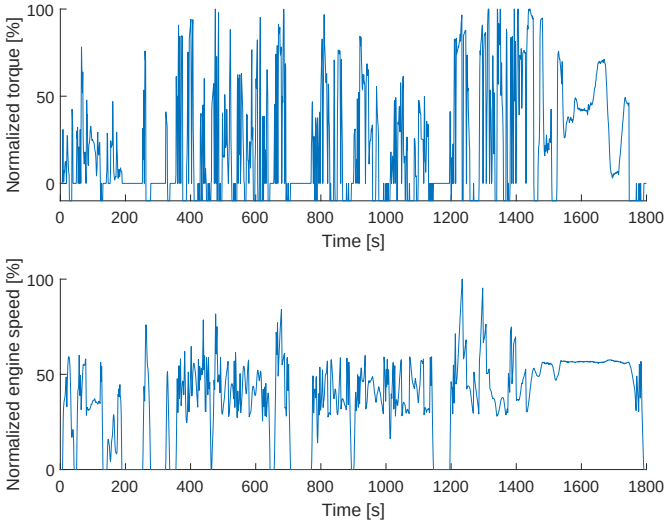

Figure 2.1: *World Harmonized Transient Cycle*

The values in Figure 2.1 need to be de-normalized in order to be tested on an engine cell. The de-normalization procedure is explained in Section B.

3

System Overview

The examined system consists of three modules: the model of the heavy duty diesel engine, the reference generator and the MPC controller. A block scheme of the modules is presented in Figure 3.1. Each module is then introduced in the sections below.

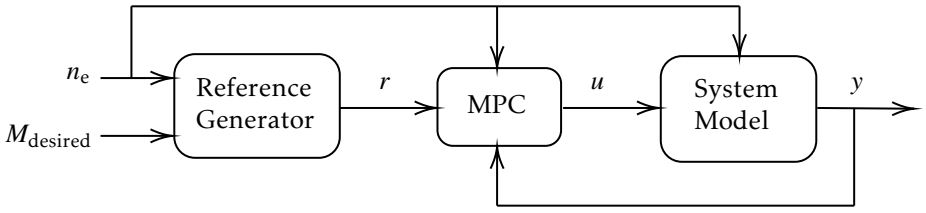

Figure 3.1: *Overview of system including reference generator, MPC controller and system model*

3.1 Model

The mean-value diesel engine model examined in this thesis is developed by *Johan Wahlström* and *Lars Eriksson* at the Department of Electrical Engineering in Linköping University. The important aspects of the model are presented below whereas the complete model description can be found in [24] and a Simulink implementation of the model and all model parameters can be downloaded from [7].

3.1.1 Model Delimitation

The following model delimitation is made:

- The actuator dynamics are neglected. As a result three states for EGR and VGT actuator positions are eliminated from the original system model.

3.1.2 Model Summary

The model structure of the diesel engine is shown in Figure 3.2.

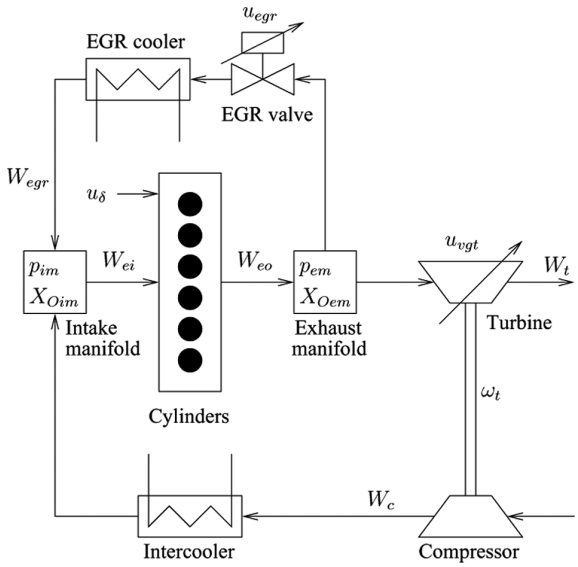

Figure 3.2: *Model structure of the diesel engine. Reprinted with permission from Wahlström and Eriksson [24]*

The model excludes both temperature dynamics and intercooler pressure drop as it has shown that neither has any notable effect on the dynamic behavior of the system. Consequently, after the model reduction described in Section 3.1.1 the model has five states collected in the state vector (3.1). The states are also described in Table 3.1.

$$x = (p_{\mathrm{im}} \quad p_{\mathrm{em}} \quad X_{\mathrm{Oim}} \quad X_{\mathrm{Oem}} \quad \omega_{\mathrm{t}})^{\mathsf{T}} \tag{3.1}$$

Table 3.1: *Description of states*

Notation	Unit	Description
p_{im}	Pa	Intake manifold pressure
p_{em}	Pa	Exhaust manifold pressure
X_{Oim}	-	Intake manifold oxygen mass fraction
X_{Oem}	-	Exhaust manifold oxygen mass fraction
ω_{t}	rad/s	Turbine rotational speed

As shown in Figure 3.2 there are three control signals, and these are collected in a control signal vector (3.2) and described in Table 3.2.

$$u = (u_\delta \quad u_{\text{egr}} \quad u_{\text{vgt}})^\intercal \tag{3.2}$$

Table 3.2: *Description of control signals*

Notation	Unit	Description
u_δ	mg/cycle	Injected amount of fuel per cylinder
u_{egr}	%	EGR control signal: closed at 0% and fully open at 100%
u_{vgt}	%	VGT control signal: closed at 0% and fully open at 100%

Additionally there is an engine rotational speed n_{e} given as an external input signal from the drive cycle. The engine rotational speed n_{e} is considered as a known disturbance, which result in the time invariant state space form (3.3).

$$\dot{x} = f(x, u, n_{\text{e}}) \tag{3.3}$$

The model covers the input ranges (3.4), (3.5) and (3.6), where p_{amb} is the ambient atmospheric pressure.

$$\begin{aligned} 0.5p_{\text{amb}} \leq p_{\text{im}} &\leq 10p_{\text{amb}} \\ 0.5p_{\text{amb}} \leq p_{\text{em}} &\leq 20p_{\text{amb}} \\ 0 \leq X_{\text{Oim}} &\leq 1 \\ 0 \leq X_{\text{Oem}} &\leq 1 \\ \frac{100\pi}{30} \leq \omega_{\text{t}} &\leq \frac{200000\pi}{30} \end{aligned} \tag{3.4}$$

$$\begin{aligned} 1 \leq u_\delta &\leq 250 \\ 0 \leq u_{\text{egr}} &\leq 100 \\ 20 \leq u_{\text{vgt}} &\leq 100 \end{aligned} \tag{3.5}$$

$$500 \leq n_{\text{e}} \leq 2000 \tag{3.6}$$

As concluded in [24] the system dynamics are modeled as (3.7) where the parameters and variables are presented in Table 3.3.

$$\frac{d}{dt}p_{\text{im}} = \frac{R_{\text{a}}T_{\text{im}}}{V_{\text{im}}}(W_{\text{c}} + W_{\text{egr}} - W_{\text{ei}}) \tag{3.7a}$$

$$\frac{d}{dt}p_{\text{em}} = \frac{R_{\text{e}}T_{\text{em}}}{V_{\text{em}}}(W_{\text{eo}} - W_{\text{t}} - W_{\text{egr}}) \tag{3.7b}$$

$$\frac{d}{dt}X_{\text{Oim}} = \frac{R_{\text{a}}T_{\text{im}}}{p_{\text{im}}V_{\text{im}}}((X_{\text{Oem}} - X_{\text{Oim}})W_{\text{egr}} + (X_{\text{Oc}} - X_{\text{Oim}})W_{\text{c}}) \tag{3.7c}$$

$$\frac{d}{dt}X_{\text{Oem}} = \frac{R_{\text{e}}T_{\text{em}}}{p_{\text{em}}V_{\text{em}}}(X_{\text{Oe}} - X_{\text{Oem}})W_{\text{eo}} \tag{3.7d}$$

$$\frac{d}{dt}\omega_{\text{t}} = \frac{P_{\text{t}}\eta_{\text{m}} - P_{\text{c}}}{J_{\text{t}}\omega_{\text{t}}} \tag{3.7e}$$

Table 3.3: *Description of parameters and variables*

Notation	Unit	Description
J_{t}	$\text{kg} \cdot \text{m}^2$	Moment of inertia for turbine
P	W	Power
R_{a}	$\text{J}/(\text{kg} \cdot \text{K})$	Ideal-gas constant for air
R_{e}	$\text{J}/(\text{kg} \cdot \text{K})$	Ideal-gas constant for exhaust
T	K	Intake manifold temperature
V	m^3	Volume
W	kg/s	Mass flow
η_{m}	-	Mechanical efficiency

Moreover, some important concepts are introduced below. All necessary variables, states and control signals are measurable through the model, meaning that there is no need for any kind of state estimation.

Engine Torque

The engine torque, M_e, is modeled using three torque components, see (3.8).

$$M_e = M_{ig} - M_p - M_{fric} \tag{3.8a}$$

$$M_{ig} = M_{ig}(u_\delta) = \frac{u_\delta 10^{-6} n_{cyl} q_{HV} \eta_{ig}}{4\pi} \tag{3.8b}$$

$$M_p = M_p(p_{im}, p_{em}) = \frac{V_d}{4\pi}(p_{em} - p_{im}) \tag{3.8c}$$

$$M_{fric} = M_{fric}(n_e) = \frac{V_d}{4\pi} 10^5 (c_{fric1}(\frac{n_e}{1000})^2 + c_{fric2}\frac{n_e}{1000} + c_{fric3}) \tag{3.8d}$$

where M_{ig} is the gross indicated torque generated from the added fuel, M_p is the pumping torque, and the friction torque M_{fric} is assumed to be a quadratic polynomial. Furthermore, n_{cyl}, q_{HV}, η_{ig}, V_d and $c_{fric1,2,3}$ are constants extracted from the model parameter data set that follows with the Simulink implementation.

Fuel Mass Flow

The fuel mass flow, W_f, can be calculated using (3.9).

$$W_f = \frac{10^{-6}}{120} u_\delta n_e n_{cyl} \tag{3.9}$$

EGR-fraction

The EGR-fraction, x_{egr}, in the intake manifolds is expressed as (3.10).

$$x_{egr} = \frac{W_{egr}}{W_c + W_{egr}} \tag{3.10}$$

Oxygen-to-fuel Ratio

The oxygen-to-fuel ratio, λ_O, in the cylinders is calculated using (3.11).

$$\lambda_O = \frac{W_{ei} X_{Oim}}{W_f (O/F)_s} \tag{3.11}$$

where $(O/F)_s$ is the stoichiometric ratio of oxygen mass to fuel mass which is given in the model parameter data set. Ideally $\lambda_O > 1$ to avoid smoke generation.

Air-to-fuel Ratio

An equivalent measurement to the oxygen-to-fuel ratio is the air-to-fuel ratio, λ, see (3.12).

$$\lambda = \frac{W_{\text{ei}} X_{\text{Oc}}}{W_{\text{f}}(\text{O/F})_{\text{s}}} = \frac{X_{\text{Oc}}}{X_{\text{Oim}}} \lambda_{\text{O}} \tag{3.12}$$

3.1.3 Control Challenges

The main dynamics and system properties are described by the intake manifold pressure, p_{im}, exhaust manifold pressure, p_{em}, and turbine rotational speed, ω_{t}. In short, the most important system properties and system control challenges are:

- Nonlinear system, see (3.7)
- From EGR valve, u_{egr}, to intake manifold pressure, p_{im}:
  - Non-minimum phase behavior, see left figure in Figure 3.3
- From VGT valve, u_{vgt}, to compressor mass flow, W_{c}:
  - Non-minimum phase behavior, see right figure in Figure 3.3
  - Overshoot
  - Sign reversal
- Coupling

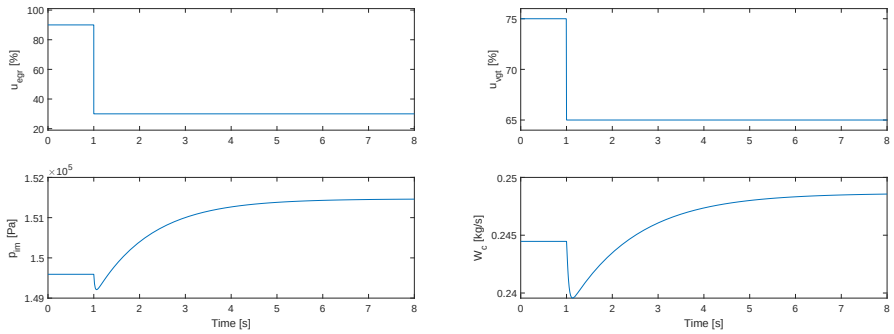

Figure 3.3: *Illustration of non-minimum phase behaviors from u_{egr} to p_{im} (left), and u_{vgt} to W_{c} (right)*

3.2 Reference Generator

The reference generator uses 2-D lookup tables to store fuel optimal steady state reference values for various desired engine torques and engine speeds. The refer-

ence values are calculated in advance using nonlinear optimization. The inputs to the optimization problems are the engine rotational speed and the desired engine torque, and with the system model it calculates the state and control signal reference values as shown in Figure 3.4 where x_{ref} and u_{ref} form the reference r seen in Figure 3.1. The method is described in more detail in Chapter 4.

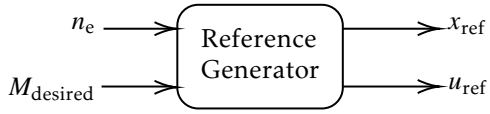

Figure 3.4: *Overview of reference generator*

3.3 Model Predictive Controller

The MPC controller linearizes the system and discretizes the continuous time optimal control problem using a direct optimal control approach and numerical integration. Thereafter the optimal control problem is as a quadratic program that can be solved with qpOASES in CasADi, see Figure 3.5.

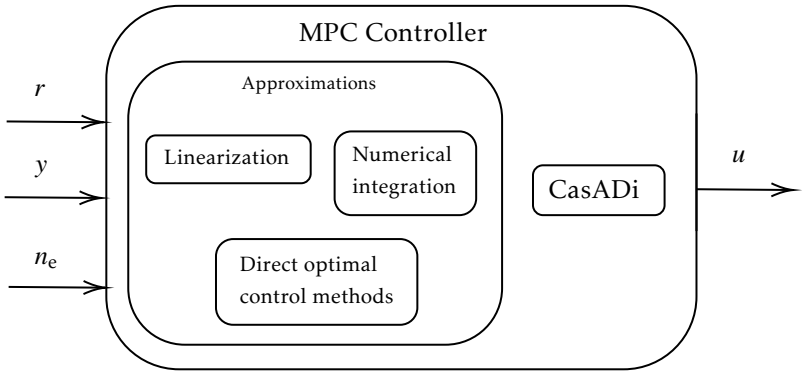

Figure 3.5: *Overview of linearization based MPC controller*

Given the reference, engine speed and fed-back outputs, the MPC controller calculates the control signal each iteration by solving an optimal control problem. The MPC controller is presented in more detail in Chapter 5.

4

Reference Generator

The purpose with the reference generator is to deliver fuel optimal stationary state and control signal reference values to the MPC controller. The reference values are calculated in advance to build an engine map, see Section 4.1, where the map facilitates an easy reference generator implementation using 2-D lookup tables in CasADi, see Section 4.2.

4.1 Engine Map Methodology

The fuel optimal stationary points are calculated for various desired torques, M_{desired}, and engine speeds, n_{e}, by solving nonlinear optimization problems, see (4.1). The different torque and engine speed values can then be used to generate an engine map, see Section 4.1.3.

$$\begin{aligned} \min_{x,u} \quad & \|x\|_{Q_1}^2 + \|u\|_{Q_2}^2 \\ \text{subject to} \quad & \dot{x} = f(x, u, n_{\text{e}}) = 0 \\ & M_{\text{e}} \geq M_{\text{desired}} \\ & \lambda(x, u) \geq 1.2 \\ & x_{\min} \leq x \leq x_{\max} \\ & u_{\min} \leq u \leq u_{\max} \end{aligned} \tag{4.1}$$

where the air-to-fuel ratio $\lambda(x, u) \geq 1.2$ is chosen for low smoke generation, M_{e} is the actual torque delivered at the stationary point, and $u_{\min}$, $u_{\max}$, $x_{\min}$ and $x_{\max}$ represent the ranges listed in (3.4) and (3.5).

In order to find fuel optimal solutions the penalization of u_δ (that is $q_{2,1}$ as pre-

sented in Section 4.1.2) is chosen large relative other states and control signals. All other states and control signals are weighted slightly in order to balance unknown system qualities and guarantee a reasonable solution. A large weight on u_δ also results in $M_e \simeq M_{\text{desired}}$ as the engine torque is highly dependent on the injected fuel, see (3.8).

The optimization problem (4.1) is nonconvex and can therefore not guarantee solvability or that the solution is a global minima. Global optimality will not be required in the reference generator as it suffices that the stationary point is fuel optimal in some sense. However, a relaxed version of (4.1) is considered if the optimizer cannot find a solution, see Section 4.1.1.

4.1.1 Relaxed Optimization Problem

The relaxed optimization problem includes the stationarity in the cost function instead of as an equality constraint, see (4.2).

$$\begin{aligned} \min_{x,u} \quad & \|x\|_{Q_1}^2 + \|u\|_{Q_2}^2 + \|\dot{x}\|_{Q_3}^2 \\ \text{subject to} \quad & M_e \geq M_{\text{desired}} \\ & \lambda(x,u) \geq 1.2 \\ & x_{\min} \leq x \leq x_{\max} \\ & u_{\min} \leq u \leq u_{\max} \end{aligned} \tag{4.2}$$

In (4.2) the penalization of the state derivatives are chosen enormous due to small derivatives near stationarity. However, the weights are successively lowered if the optimizer still has difficulties finding a solution. The relaxation allows solutions where stationarity is almost satisfied ($\dot{x} \approx 0$) or even solutions without stationarity depending on the design parameters, see Section 4.1.2.

4.1.2 Design Parameters

The design parameters for (4.1) and (4.2) are the weight matrices Q_1, Q_2 and Q_3.

$$Q_1 = \begin{bmatrix} q_{1,1} & 0 & 0 & 0 & 0 \\ 0 & q_{1,2} & 0 & 0 & 0 \\ 0 & 0 & q_{1,3} & 0 & 0 \\ 0 & 0 & 0 & q_{1,4} & 0 \\ 0 & 0 & 0 & 0 & q_{1,5} \end{bmatrix}, \quad Q_3 = \begin{bmatrix} q_{3,1} & 0 & 0 & 0 & 0 \\ 0 & q_{3,2} & 0 & 0 & 0 \\ 0 & 0 & q_{3,3} & 0 & 0 \\ 0 & 0 & 0 & q_{3,4} & 0 \\ 0 & 0 & 0 & 0 & q_{3,5} \end{bmatrix}$$

$$Q_2 = \begin{bmatrix} q_{2,1} & 0 & 0 \\ 0 & q_{2,2} & 0 \\ 0 & 0 & q_{2,3} \end{bmatrix}$$

These matrices represent the penalization of the states, control signals and state

derivatives in the cost function. The weight matrices are symmetric and positive-definite to penalize each term separately.

The design parameters are normalized into a fairly uniform scale to account for the different magnitudes of the states and control signals. The normalization considers a squared average of the minimum and maximum values, which is illustrated in the example (4.3).

$$q_{1,1} = \frac{q_1}{(\frac{x_{1,\min}+x_{1,\max}}{2})^2} \tag{4.3}$$

4.1.3 Engine Map

Solving (4.1) and (4.2) for various desired torques and engine speeds result in the engine map presented in Figure 4.1, where the maximum stationary torque curve follows from Figure B.1. Each solution represents different pairs of reference values (x_{ref} and u_{ref}).

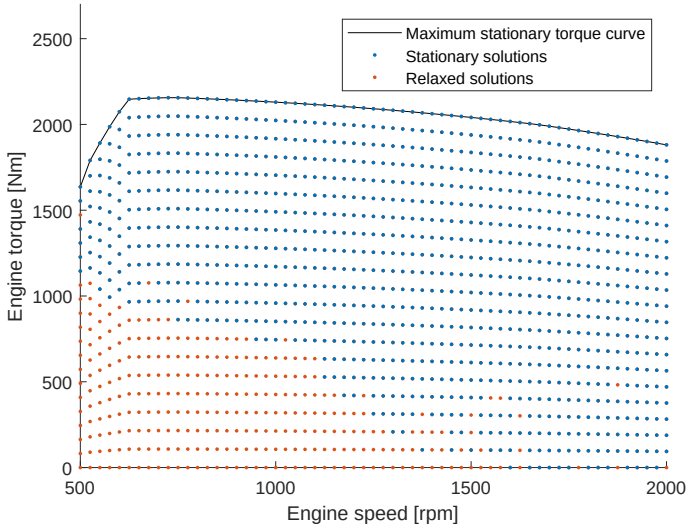

Figure 4.1: *Engine map: solutions to* (4.1) *and* (4.2)

4.2 Lookup Tables

The reference values in Figure 4.1 are stored in separate 2-D lookup tables in CasADi. In order to match the sizes of the tables the engine torque is normalized with respect to the maximum stationary torque curve, see Figure B.1. The lookup table data along with the state derivatives are presented in Chapter C, but the intake manifold pressure data, p_{im}, is presented in Figure 4.2 as an illustrative example.

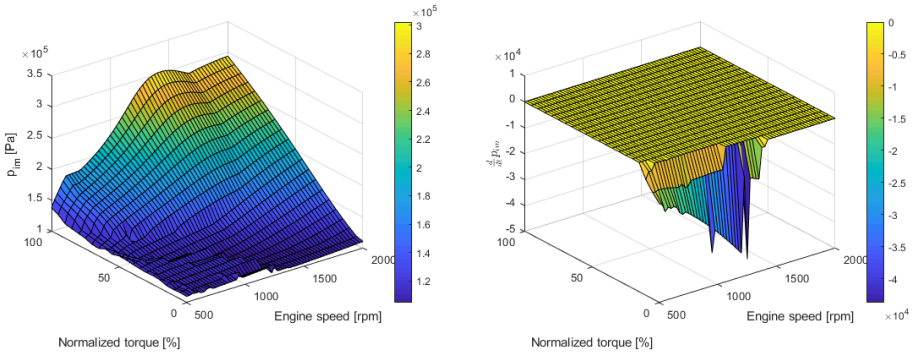

Figure 4.2: *Illustration of table data (left) and its derivative (right)*

The lookup tables evaluate the sampled data and approximate two-dimensional functions for all states and control signals using linear interpolation. The inputs to the lookup tables are the normalized desired torque $M_{\text{desired}}^{\text{norm}}$ and actual engine speed n_{e} and the outputs are the interpolated reference values, see Figure 4.3.

Figure 4.3: *Inputs and outputs to the lookup tables*

The reference generator, see Figure 3.4, converts the input M_{desired} to the lookup table input $M_{\text{desired}}^{\text{norm}}$ using the maximum torque curve.

4.2.1 Negative Torque Inputs

When using WHTC as test cycle there are torque inputs with negative values. During such instances the controller is bypassed and the lowest amount of fuel (namely u_δ = 1mg/cycle for this model) is provided to the engine while u_{egr} and u_{vgt} remain the same.

4.2.2 Relaxed Solutions

It is shown in Figure 4.2 that stationarity is lost when relaxing the optimization problem. This is mostly in the low torque ranges and it is likely that: stationary points in these ranges do not exist at all, that there is no existing stationary solution for the desired torque or that the model is not formulated well for low torque ranges.

A reoccurring relaxed solution in the WHTC is the solution for 0% torque at an engine speed of 500 rpm. An engine simulation using the solution as input follows in Figure 4.4 and Figure 4.5.

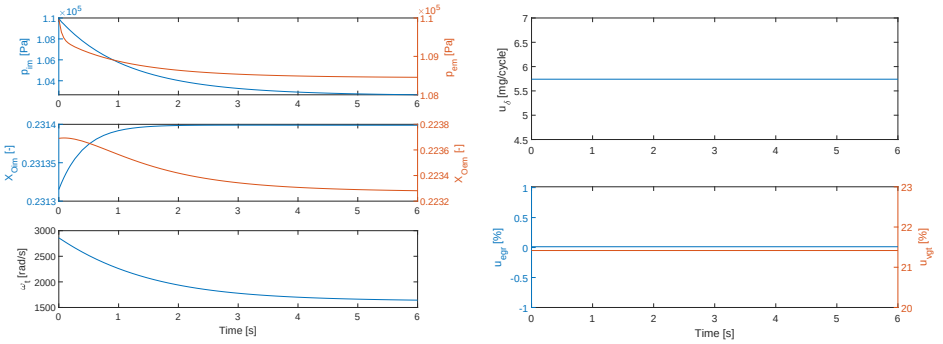

Figure 4.4: *Simulation of 0% torque at 500 rpm: states and control signals*

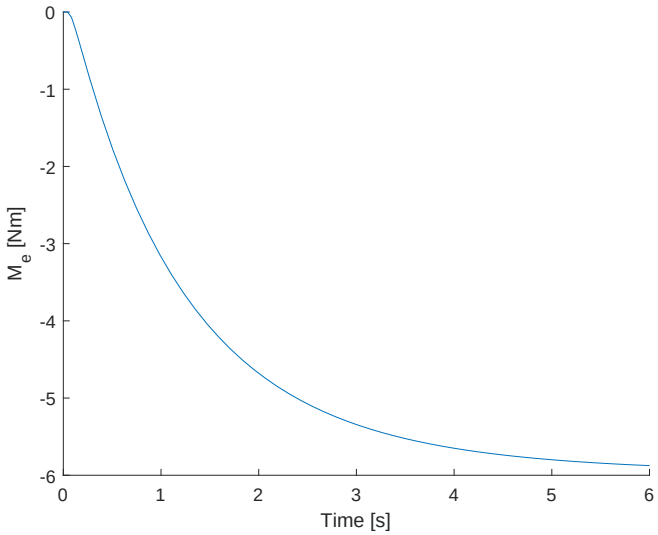

Figure 4.5: *Simulation of 0% torque at 500 rpm: engine torque*

Figure 4.4 and Figure 4.5 show that the engine stabilizes itself around another stationary solution with a small negative torque. From (3.8) the engine torque M_e is expressed as a function of the pumping losses, $p_{em} - p_{im}$, for constant u_δ and n_e. Consequently the engine torque stabilizes when the pumping losses become constant in steady state.

For the non-stationary relaxed solutions it is deemed sufficient that the solutions are close to stationary.

5

Model Predictive Control

This chapter covers the design of the linearization based state feedback MPC controllers, see Section 5.1, as well as the measurements of controller performance, see Section 5.2.

5.1 Control Designs

The MPC controllers aim to solve continuous time optimization problems on the form of (5.1) for a given time horizon T.

$$\begin{aligned} \min_{u(\cdot)} \quad & \int_0^T \ell_c(x(t), u(t))dt + V_f(x(T)) \\ \text{subject to} \quad & x(0) = x_0 \\ & \dot{x}(t) = f_c(x(t), u(t)), \quad t \in [0, T] \\ & g(x(t), u(t)) \leq 0, \quad t \in [0, T] \\ & x_{\min} \leq x(t) \leq x_{\max}, \quad t \in [0, T] \\ & u_{\min} \leq u(t) \leq u_{\max}, \quad t \in [0, T] \end{aligned} \tag{5.1}$$

The optimization problem (5.1) is discretized using direct multiple shooting due to the infinite-dimensional complexity of continuous time optimal control problems. The methods (2.3) and (2.4) yield the discretized optimal control problem (5.2).

$$
\begin{aligned}
\min_{\boldsymbol{x},\boldsymbol{u}} \quad & \textstyle\sum_{k=0}^{N-1} h\ell_c(x(hk), u(hk)) + V_f\left(x(Nh)\right) \\
\text{subject to} \quad & x(0) = x_0 \\
& x(h(k+1)) = f_c(x(hk), u(hk)), \quad \text{for } k = 0, 1, \ldots, N-1 \\
& g(x(hk), u(hk)) \leq 0, \quad \text{for } k = 0, 1, \ldots, N-1 \\
& x_{\min} \leq x(hk) \leq x_{\max}, \quad \text{for } k = 0, 1, \ldots, N-1 \\
& u_{\min} \leq u(hk) \leq u_{\max}, \quad \text{for } k = 0, 1, \ldots, N-1
\end{aligned}
\tag{5.2}
$$

where h is the step size and $N = T/h$ is the prediction horizon. The following subsections will present the implemented MPC controllers as modified versions of (5.2).

5.1.1 Linearization Based MPC

The linearization based MPC (LMPC) linearizes the nonlinear system dynamics (3.7) once about a constant linearization point (a, b). Using (2.10), the linearized system is expressed as (5.3).

$$
\dot{\tilde{x}} \approx \tilde{f}(x(hk), u(hk)) = A(x(hk) - a) + B(u(hk) - b) + K \tag{5.3}
$$

where A, B and K are constant matrices. The Forward Euler integrator, see Algorithm 1, is considered for the numerical simulation of the system dynamics, since when studying linearized systems the Forward Euler integration method is exact. This results in the MPC design (5.4) where the output comes from state feedback $y = x$.

$$
\begin{aligned}
\min_{\boldsymbol{x},\boldsymbol{u}} \quad & \textstyle\sum_{k=0}^{N-1} h\Big[\|y(hk) - x_{\text{ref}}(hk)\|^2_{Q_1} + \|u(hk) - u_{\text{ref}}(hk)\|^2_{Q_2} + \ldots \\
& \qquad \|u(hk) - u(h(k-1))\|^2_{Q_3}\Big] + h\|y(Nh) - x_{\text{ref}}(Nh)\|^2_{Q_4} \\
\text{subject to} \quad & x(0) = x_0 \\
& x(h(k+1)) = x(hk) + h\tilde{f}(x(hk), u(hk)), \text{ for } k = 0, 1, \ldots, N-1 \\
& y(hk) = x(hk), \quad \text{for } k = 0, 1, \ldots, N-1 \\
& y_{\min} \leq y(hk) \leq y_{\max}, \quad \text{for } k = 0, 1, \ldots, N \\
& u_{\min} \leq u(hk) \leq u_{\max}, \quad \text{for } k = 0, 1, \ldots, N-1
\end{aligned}
\tag{5.4}
$$

where the design utilizes the concepts for reference tracking and integral action presented in Section 2.4.1 as well as utilizing the linearized system (5.3) for the forward Euler integration.

In (5.4) it can also be noted that:

- The integral action can be removed by neglecting the term $\|u(hk) - u(h(k-1))\|^2_{Q_3}$ from the cost function.
- The reference tracking can consider both constant references and preview.

Design Parameters

The weight matrices Q_1, Q_2, Q_3 and Q_4 in (5.4) are chosen as symmetric and positive definite.

$$Q_1 = \begin{bmatrix} q_{1,1} & 0 & 0 & 0 & 0 \\ 0 & q_{1,2} & 0 & 0 & 0 \\ 0 & 0 & q_{1,3} & 0 & 0 \\ 0 & 0 & 0 & q_{1,4} & 0 \\ 0 & 0 & 0 & 0 & q_{1,5} \end{bmatrix}, \quad Q_2 = \begin{bmatrix} q_{2,1} & 0 & 0 \\ 0 & q_{2,2} & 0 \\ 0 & 0 & q_{2,3} \end{bmatrix}$$

$$Q_3 = \begin{bmatrix} q_{3,1} & 0 & 0 \\ 0 & q_{3,2} & 0 \\ 0 & 0 & q_{3,3} \end{bmatrix}, \quad Q_4 = \begin{bmatrix} q_{4,1} & 0 & 0 & 0 & 0 \\ 0 & q_{4,2} & 0 & 0 & 0 \\ 0 & 0 & q_{4,3} & 0 & 0 \\ 0 & 0 & 0 & q_{4,4} & 0 \\ 0 & 0 & 0 & 0 & q_{4,5} \end{bmatrix}$$

This structure of the weight matrices makes the cost function quadratic and convex, resulting in a convex optimization problem that can be solved as a quadratic program. The weight matrices are normalized with respect to the square of the average average of the minimum and maximum values as illustrated in (4.3).

Additional design parameters for MPC controller design (5.4) include the sampling rate T_s, the step size h and the horizons N and T, where $N = T/h$.

5.1.2 Successive Linearization Based MPC

The successive linearization based MPC (SLMPC) controller follows the same structure as in Section 5.1.1. The difference is that the linearized system becomes time dependent because of the time dependent linearization point $(a(hk), b(hk))$, see (5.5).

$$\dot{\tilde{x}} \approx \tilde{f}(x(hk), u(hk)) = A(hk)(x(hk) - a(hk)) + B(hk)(u(hk) - b(hk)) + K(hk) \quad (5.5)$$

The controller structure is the same as shown in (5.4) but using (5.5) instead of (5.3) for the Forward Euler integration.

5.2 Measurements of Controller Performance

The measurements of controller performance are constructed with respect to the aim of the thesis, that is reference tracking of the engine torque and total fuel consumption, but also the total work required during the test cycle is investigated. The measurements are integrated over time using trapezoidal numerical integration (`trapz` in MATLAB) for a given cycle time T_{cycle}.

Closed rack motoring, that is negative torque values, are excluded from the controller performance measurements as the controller is bypassed during closed rack motoring as described in Section 4.2.1.

5.2.1 Tracking Error

The tracking error of the torque, e_{M_e}, is calculated with (5.6).

$$e_{M_e} = \frac{1}{T_{\text{cycle}}} \int_0^{T_{\text{cycle}}} |M_{\text{desired}} - M_e| dt \tag{5.6}$$

5.2.2 Fuel Consumption

The total consumed fuel mass, m_f, is calculated using the measurement for fuel mass flow, W_f, according to (5.7).

$$m_f = \int_0^{T_{\text{cycle}}} W_f dt \tag{5.7}$$

5.2.3 Mechanical Work

The total mechanical work, E_m, from the engine is calculated using the actual torque and the engine speed according to (5.8).

$$E_m = \int_0^{T_{\text{cycle}}} M_e \omega_e dt = \frac{30}{\pi} \int_0^{T_{\text{cycle}}} M_e n_e dt \tag{5.8}$$

6
Results

This chapter presents the results of the MPC controllers in Section 5, see (5.4) with (5.3) and (5.5). The following controllers are considered:

- LMPC with linearization about a single linearization point corresponding to 80 kW mechanical power at an engine speed of 1200 rpm, see Section 6.2
- SLMPC with linearization about current operating point ($x(t)$ and $u(t)$), see Section 6.3
- SLMPC with linearization about reference values (x_{ref} and u_{ref}), see Section 6.4

Transient responses, ramp responses and sinusoidal responses are carried out for each controller design to give insight into the controller performance. The studied responses start from steady state and in discrete time calculations they can be considered as unit steps. For each response, the oxygen-to-fuel ratio and EGR-fraction are logged in addition to the engine torque, states and control signals.

Moreover, the controllers are evaluated in Section 6.5 using the measurements (5.6), (5.7) and (5.8) when simulating the diesel engine with the de-normalized WHTC data presented in Chapter B.

6.1 Controller Design

This section covers the resulting design parameters and the effects of preview and integral action.

6.1.1 Design Parameters

The controllers in the following subsections are designed with the sampling rate $T_s = 0.01$ s, step size $h = T_s = 0.01$ s and time horizon $T = 0.4$ s. Equivalently, the prediction horizon for the discretized optimization problem is $N = T/h = 40$ samples. The weight matrices for the controller designs are presented in Chapter D and a discussion regarding the choice of design parameters follows in Section 7.1.

6.1.2 Time Horizon using Preview

Figure 6.1 presents a transient response comparison of different time horizons T for the LMPC controller described in Section 6.2.

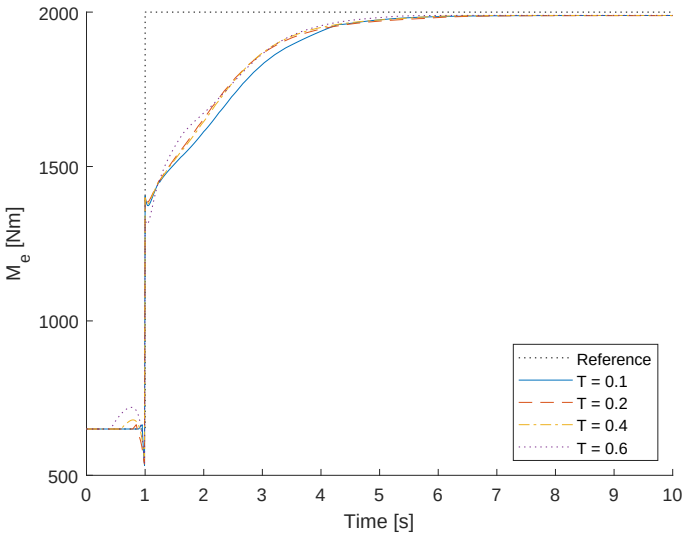

Figure 6.1: *Effect of time horizon using LMPC with preview: transient from 650 Nm to 2000 Nm at 1200 rpm*

6.1.3 Integral Action

To illustrate the effect of the integral action, the MPC controller in Section 6.3 with preview is considered in Figure 6.2. It is shown that the integral action has almost no effect on neither the torque generation nor tracking of the state references. However, the control signals become less oscillatory. The effect of the

integral action is investigated further in Table 6.1. All test responses presented in this chapter use integral action unless stated otherwise.

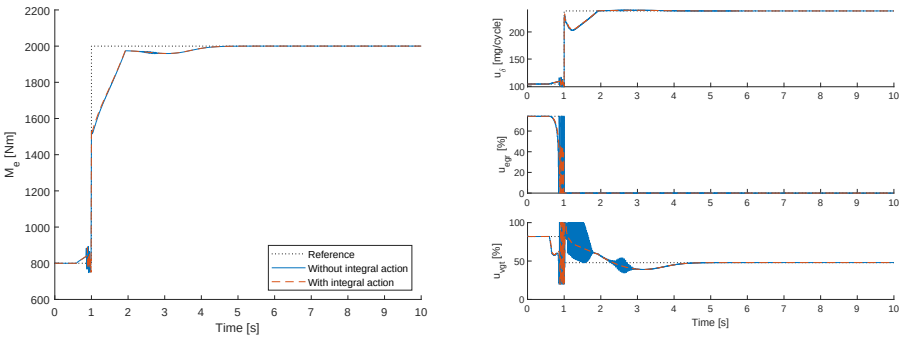

Figure 6.2: *Effect of integral action using SLMPC about current operating point: transient from 800 Nm to 2000 Nm at 1200 rpm*

6.2 Linearization Based MPC

The nonlinear system is linearized about the linearization points that corresponds to 80 kW mechanical power at an engine speed of 1200 rpm (also denoted LMPC), which is a common operating range for heavy duty vehicles. The linearization points are almost equivalent to an engine torque of 637 Nm. The test responses are executed both with and without preview as presented in the subsections below.

6.2.1 Transient Response

Two transient responses are considered: a small transient from 800 Nm to 900 Nm, see Figure 6.3, and a large transient from 650 Nm to 2000 Nm, see Figure 6.4. The engine speed remains constant during the transients.

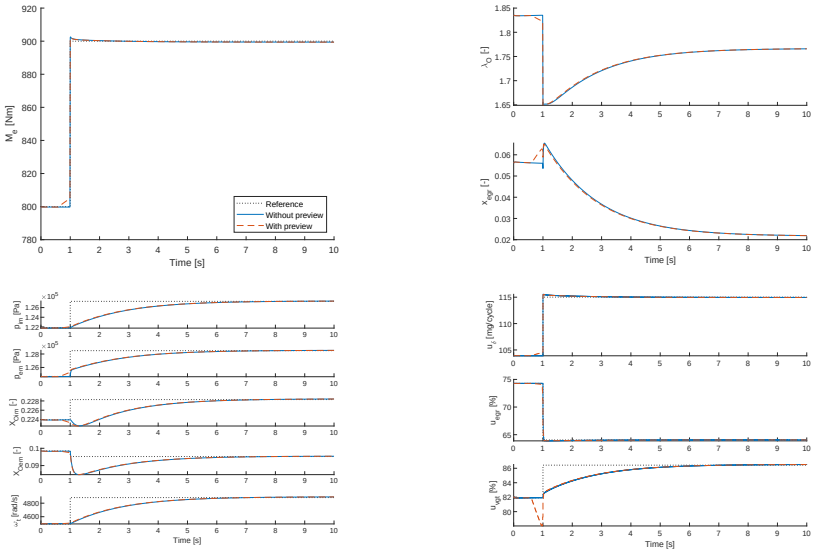

Figure 6.3: *Transient from 800 Nm to 900 Nm at 1200 rpm:* LMPC

Figure 6.3 shows that the controller reacts to small changes in the load almost instantaneously by providing more fuel and using more oxygen for the combustion (seen from the decreased X_{Oem}). It can also be noted that λ_{O} remains above the ideal value of 1, resulting in no smoke generation.

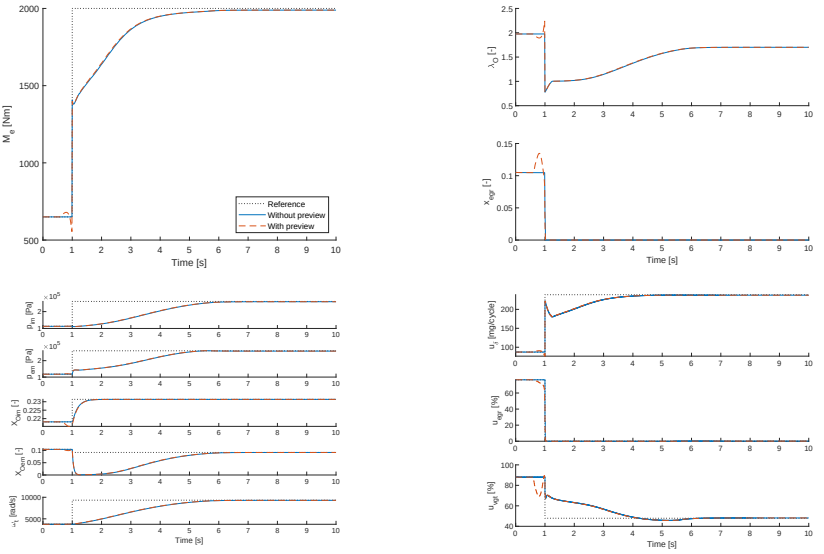

Figure 6.4: *Transient from 650 Nm to 2000 Nm at 1200 rpm:* LMPC

A bottleneck for the combustion in the larger transient in Figure 6.4 is the lack of oxygen as seen from X_{Oem} decreasing to zero. By closing the EGR actuator, more energy will instead be provided to the turbine to increase its rotational speed ω_{t}. This results in more air being fed to the engine, and in combination with less exhaust gas recirculation this leads to more available oxygen (and an increasing X_{O}) but it is not enough to avoid smoke generation completely since $\lambda_{\mathrm{O}} < 1$ for less than a second. It takes some time to build up the pressures p_{im} and p_{em} as well as the turbine rotational speed ω_{t} before the engine is able to deliver the desired torque. However, a small stationary error of approximately 10 Nm is noted in the torque tracking using LMPC.

6.2.2 Ramp Response

The ramp response covers a constantly increasing unit ramp which increases 200 Nm per second (that is 2 Nm per sample), see Figure 6.5. The ramp response shows a small stationary error in the torque response.

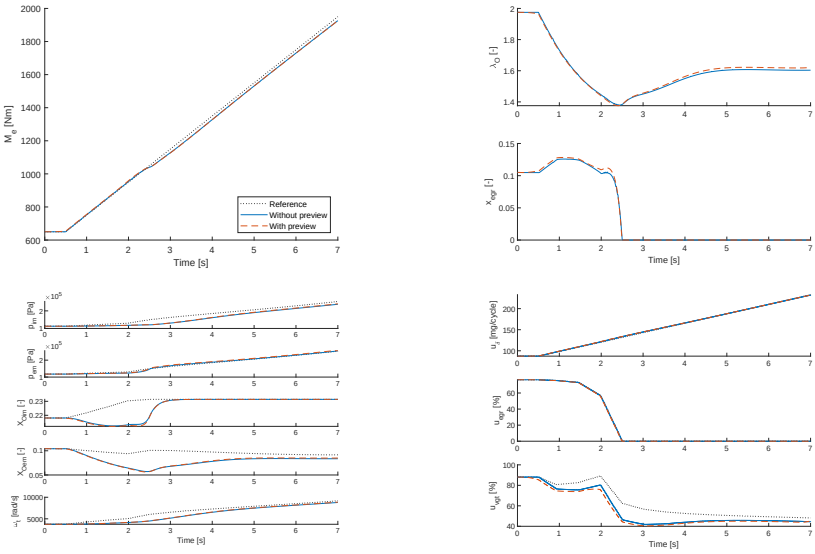

Figure 6.5: *Ramp response at 1200 rpm: LMPC*

6.2.3 Sinusoidal Response

The controller is tested using a sinusoidal reference $M_{\text{desired}} = 1000 + 500 \sin\left(\frac{\pi}{2}t\right)$ Nm, see Figure 6.6.

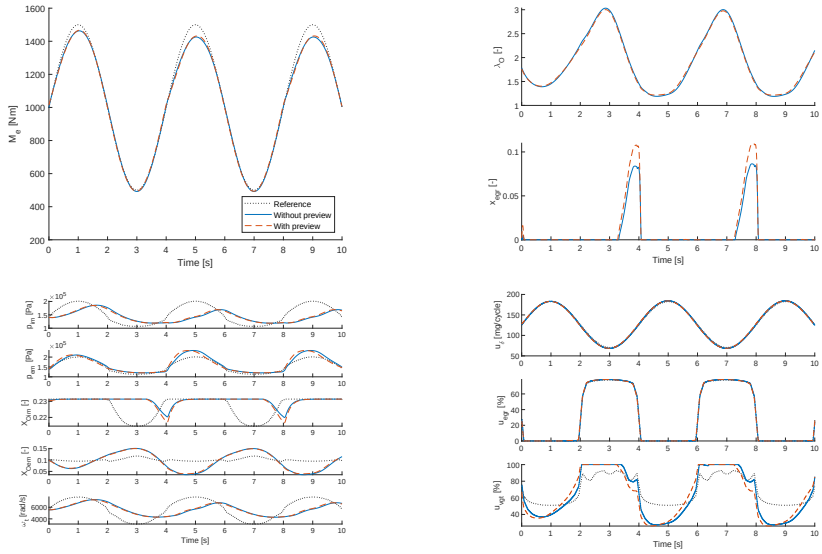

Figure 6.6: *Sinusoidal response at 1200 rpm:* LMPC

6.2.4 Drawback

The drawback with linearizing the system only once is that the system dynamics risk becoming inaccurate far from the linearization point. This is illustrated in Figure 6.7 where a lower engine speed of 700 rpm is considered. It shows that the LMPC is unable to deliver the desired torque.

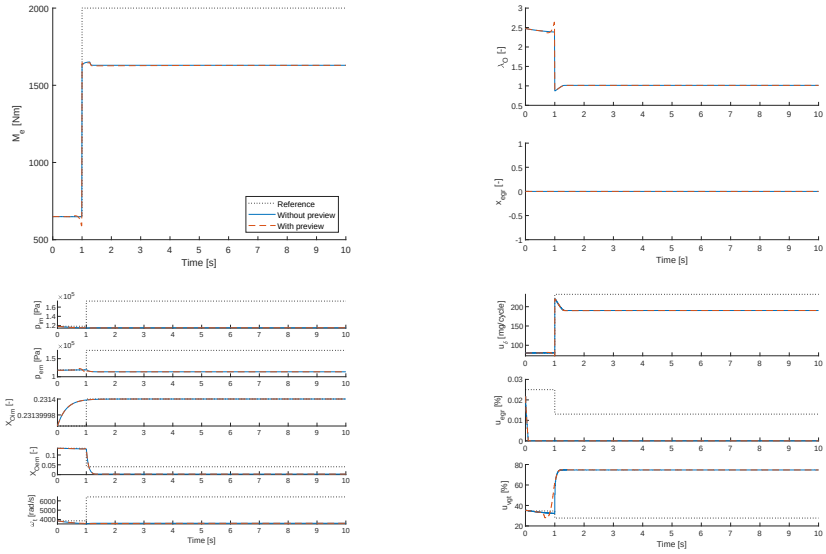

Figure 6.7: *Transient from 650 Nm to 2000 Nm at 700 rpm:* LMPC

6.3 Successive Linearization Based MPC about Current Operating Point

The idea with the succesive LMPC about current operating point (also denoted SLMPC: current) is that these signals are easily accessible since they are measured every iteration. The test responses are presented in the subsections below.

6.3.1 Transient Response

Similar to the LMPC two different transients are considered, see Figure 6.8 and Figure 6.9. No stationary error are noted for the large transient, but an oscillatory behavior in the control signals is introduced when using preview.

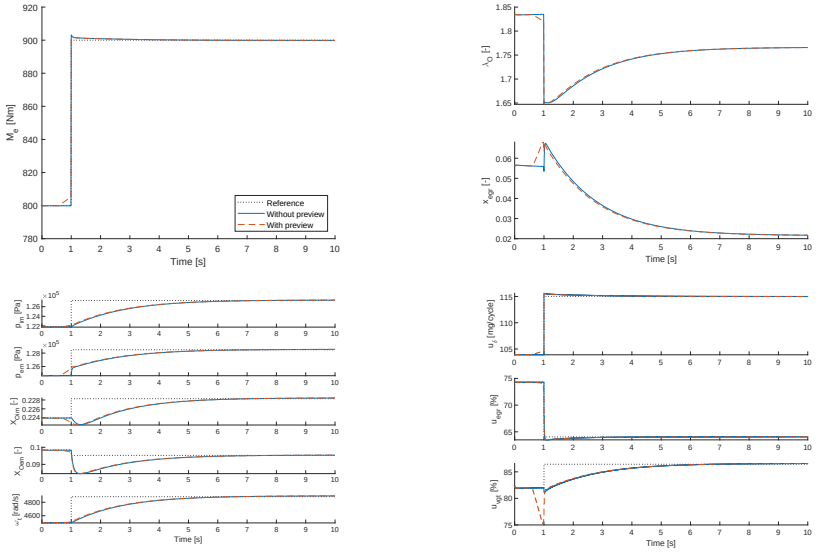

Figure 6.8: *Transient from 800 Nm to 900 Nm at 1200 rpm: SLMPC about current operating point*

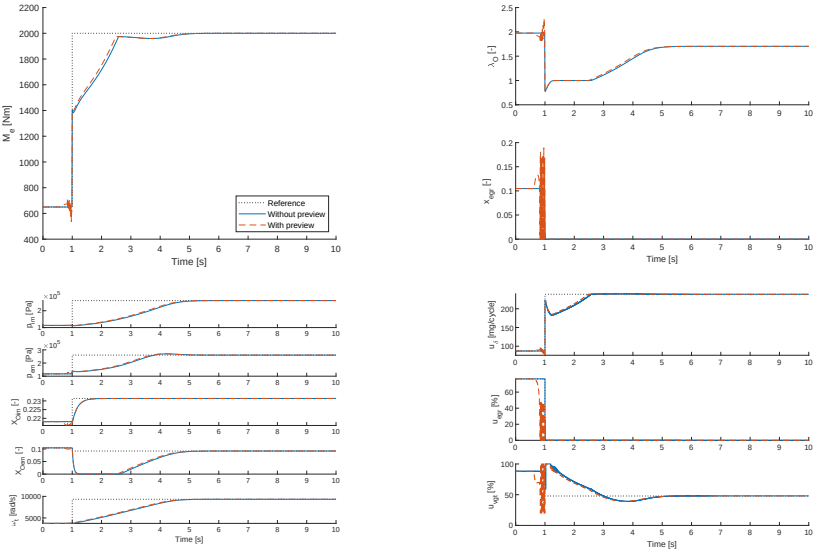

Figure 6.9: *Transient from 650 Nm to 2000 Nm at 1200 rpm: SLMPC about current operating point*

6.3.2 Ramp Response

The same ramp response as studied earlier is considered, namely a constantly increasing unit ramp which increases 200 Nm per second, see Figure 6.10.

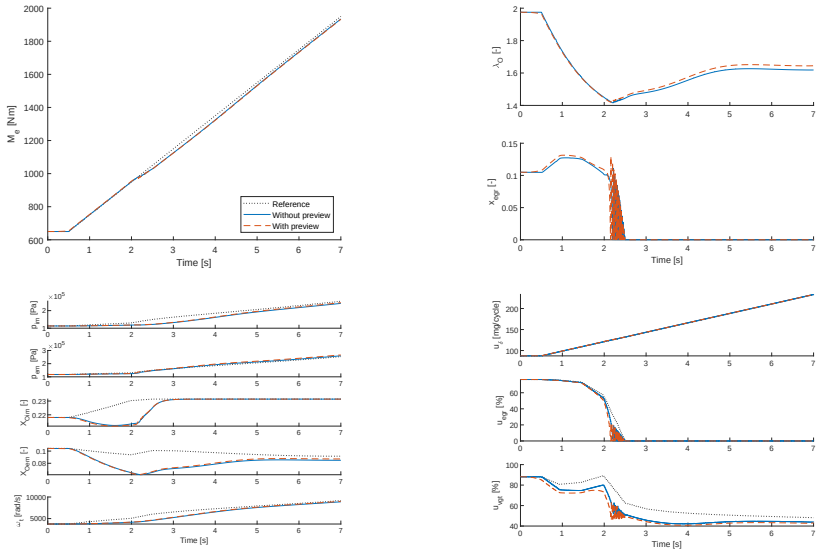

Figure 6.10: *Ramp response at 1200 rpm: SLMPC about current operating point*

6.3.3 Sinusoidal Response

The controller is tested using a sinusoidal reference $M_{\text{desired}} = 1000 + 500 \sin\left(\frac{\pi}{2}t\right)$ Nm, see Figure 6.11.

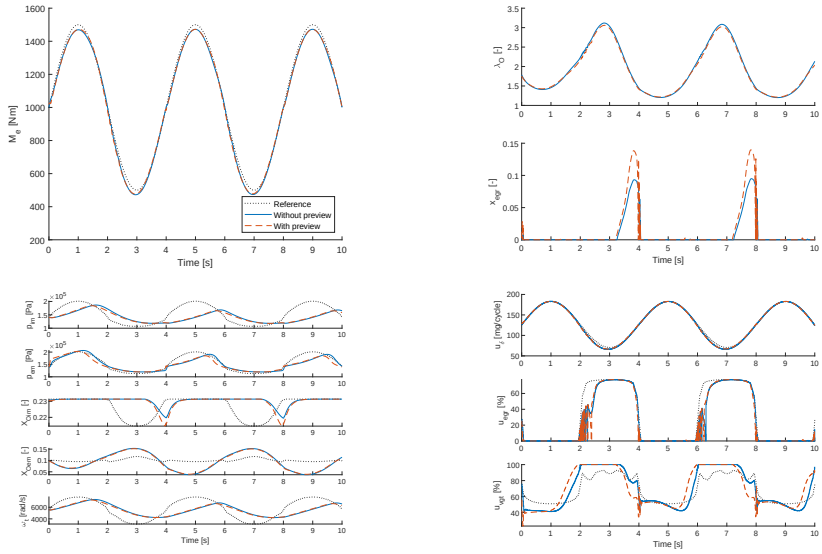

Figure 6.11: *Sinusoidal response at 1200 rpm: SLMPC about current operating point*

6.4 Successive Linearization Based MPC about Reference Values

Another approach is to linearize the system about the reference values (x_{ref} and u_{ref}) that follow from the reference generator (also denoted SLMPC: reference). Oftentimes these values are stationary points unless the controller is dealing with the relaxed solutions covered in Section 4.2.2.

6.4.1 Transient Response

The same transients as earlier are considered, see Figure 6.12 and Figure 6.13. There is no stationary error.

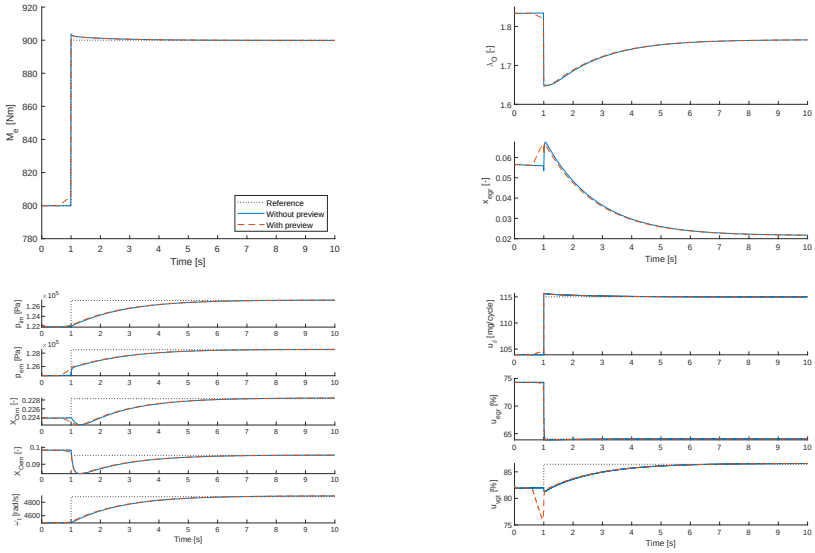

Figure 6.12: *Transient from 800 Nm to 900 Nm at 1200 rpm: SLMPC about reference values*

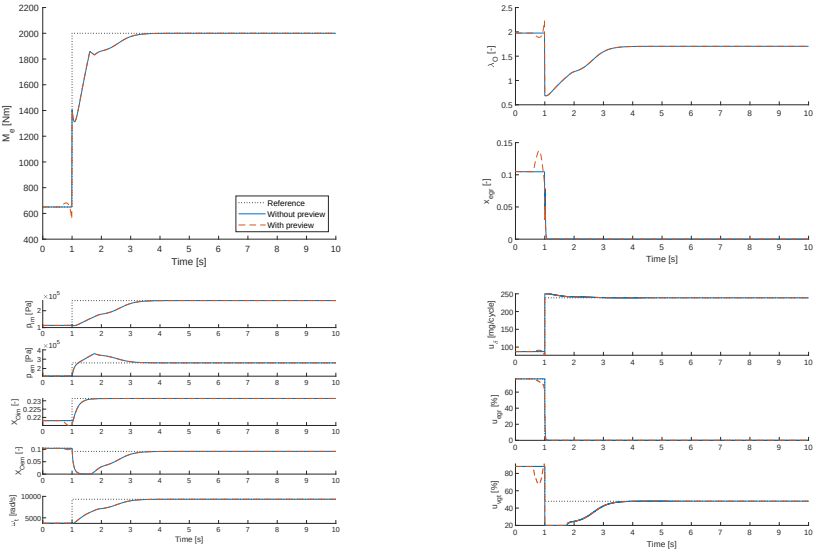

Figure 6.13: *Transient from 650 Nm to 2000 Nm at 1200 rpm: SLMPC about reference values*

6.4.2 Ramp Response

The same ramp response as studied earlier is considered, namely a constantly increasing unit ramp which increases 200 Nm per second, see Figure 6.14.

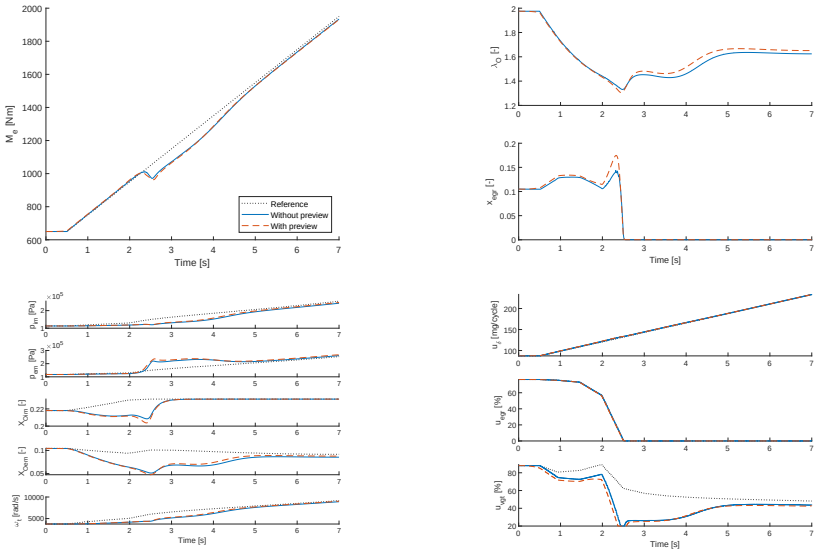

Figure 6.14: *Ramp response at 1200 rpm: SLMPC about reference values*

6.4.3 Sinusoidal Response

The controller is tested using the previously studied sinusoidal reference $M_{\text{desired}} = 1000 + 500 \sin\left(\frac{\pi}{2}t\right)$ Nm, see Figure 6.15.

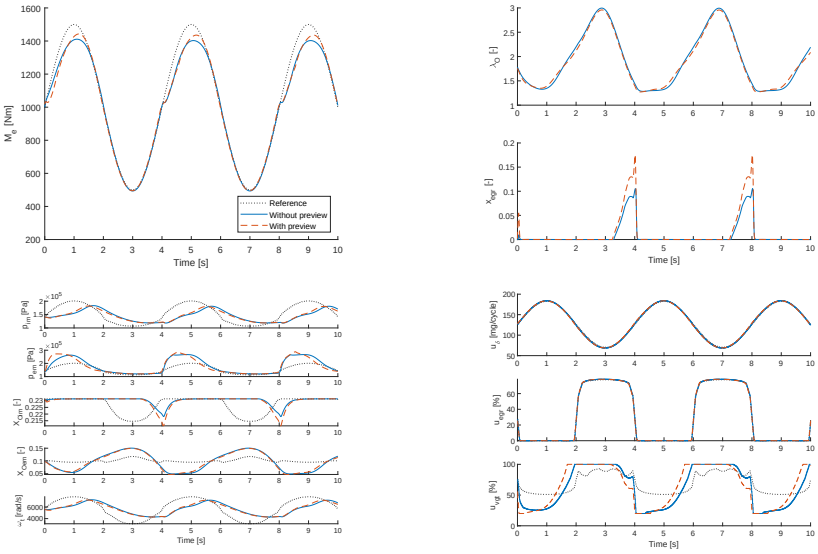

Figure 6.15: *Sinusoidal response at 1200 rpm: SLMPC about reference values*

6.5 Evaluation of Controller Performance

The examined MPC controllers are evaluated using the de-normalized WHTC data presented in Figure B.2. The second-by-second data points are interpolated using shape-preserving piecewise cubic interpolation (`pchip`) to resemble continuous signals. The results using the measurements (5.6), (5.7) and (5.8) are presented in Table 6.1 where tracking error, fuel consumption and mechanical work during closed rack motoring are neglected.

Table 6.1: *Controller performance data where IA and P denote integral action and preview respectively*

Controller	IA	P	e_{M_e} [Nm]	m_f [kg]	E_m [kWh]	$\frac{m_f}{E_m}$ [g/kWh]
LMPC	-	-	10.2659	6.1227	2535.9	2.4144
	✓	-	10.3587	6.1217	2535.5	2.4144
	-	✓	11.4520	6.1130	2531.7	2.4146
	✓	✓	11.5868	6.1116	2531.1	2.4146
SLMPC: current	-	-	N/A	N/A	N/A	N/A
	✓	-	N/A	N/A	N/A	N/A
	-	✓	N/A	N/A	N/A	N/A
	✓	✓	N/A	N/A	N/A	N/A
SLMPC: reference	-	-	9.2671	6.1634	2536.7	2.4297
	✓	-	9.2742	6.1636	2536.7	2.4298
	-	✓	9.1646	6.1628	2538.2	2.4281
	✓	✓	9.1696	6.1629	2538.2	2.4281

The SLMPC about current operating point is unable to provide reasonable results when testing with WHTC. A discussion regarding this follows in Section 7.2. A visual comparison of the torque tracking follows in Figure 6.16 and in the zoomed in version in Figure 6.17.

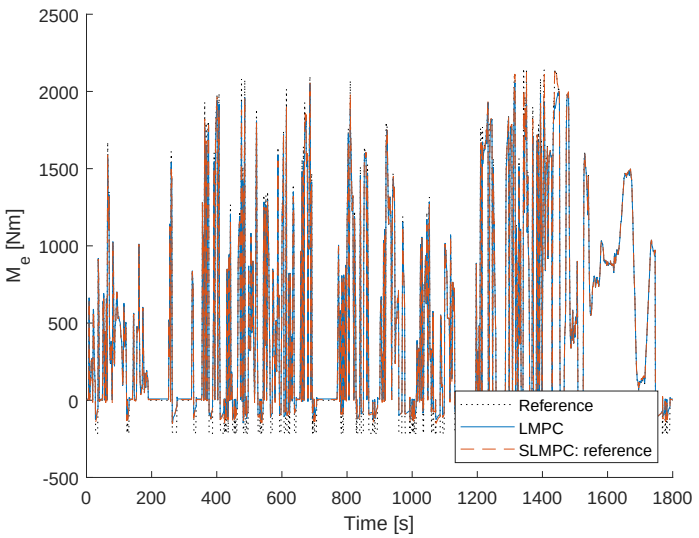

Figure 6.16: *WHTC torque tracking comparison between LMPC and SLMPC using integral action. Negative torque values can be ignored (closed rack motoring)*

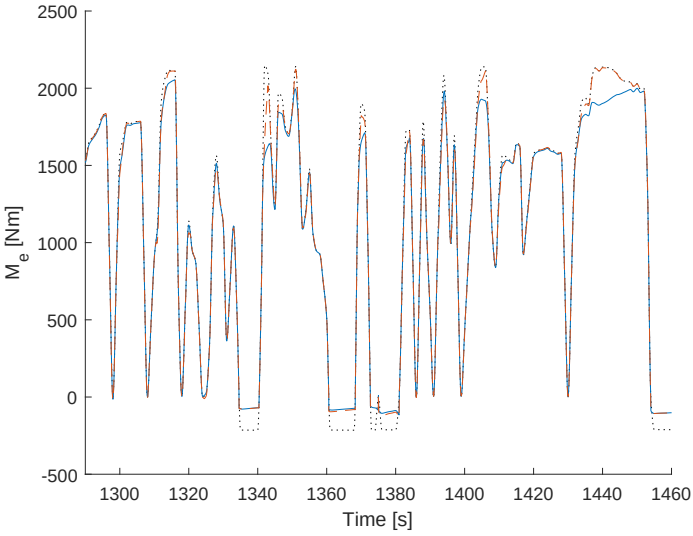

Figure 6.17: *Zoom of Figure 6.16 from 1290 to 1460 s*

7

Discussion and Conclusions

This chapter contains a discussion regarding some important design concepts and the controller performance based on the results in Chapter 6. Finally, some future work ideas are presented followed by the conclusions of the thesis.

7.1 Design Concepts

This section covers brief discussions about some important MPC design parameters and design concepts.

7.1.1 Weight Matrices

As shown in (3.8) the engine torque is a function of the injected fuel u_δ and the pumping losses $p_{\text{em}} - p_{\text{im}}$ for a known constant engine speed n_{e}. To accommodate acceptable reference tracking of the engine torque it is therefore important to have satisfactory tracking of u_δ, p_{im} and p_{em} respectively. However, a threshold for good tracking of the pressure comes from the turbocharger as its functionality is to boost the intake air pressure, hence adequate tracking of ω_{t} is desired as well. Consequently, the non-normalized weights on u_δ, p_{im}, p_{em} and ω_{t} are chosen large relative other weights, see Chapter D.

7.1.2 Sampling Rate

A large sample rate leads to slow response to disturbances while a faster sample rate result in faster response to disturbances but also yields a more computationally heavy MPC controller. The sampling rate $T_{\text{s}} = 0.01$ s is chosen partly as a compromise between fast response time and computational complexity, and

partly because the diesel engine is a fast system as can be seen from the test responses in Chapter 6.

Furthermore, a too high sample rate renders the studied continuous time MPC controllers unfeasible, for instance the LMPC controller cannot guarantee to find solutions if the sample rate is chosen as $T_s \geq 0.03$ s, and the SLMPC controller with linearization about reference values cannot guarantee solutions if the sample rate is chosen as $T_s \geq 0.08$ s.

7.1.3 Time Horizon

Figure 6.1 shows that an increased time horizon does not necessarily result in significantly better torque reference tracking. Ideally the time horizon should be chosen to cover the significant dynamics in the response, but the computational complexity of the controller increases exponentially with the time horizon. For instance, when considering the large transient responses in Figure 6.4, Figure 6.9 and Figure 6.13 it can be noted that a time horizon of approximately 5-6 s is ideal to cover most of the dynamics. However, with the short sampling rate of $T_s = 0.01$ the optimization problem (5.4) would have around 4000-4800 decision variables for a time horizon of 5-6 s. As a result, longer time horizons are not considered due to the complexity, but for the sake of comparison the time horizon $T = 0.4$ s is chosen due to its relatively short computational time.

7.1.4 Preview

The result of MPC with preview highly depends on the selected time horizon. The higher time horizon, the earlier the controller tries to adapt to the future reference values. A slight improvement in torque reference tracking using preview is shown in Figure 6.15, but in other responses it seems that the reference tracking is worse as the engine manages to react swiftly enough even without preview and a too early adaption only results in worse performance.

A better comparison follows from the results in Table 6.1. A consequence of using preview is the reduced fuel consumption. However, for LMPC it also results in worse tracking error while SLMPC controller with linearization about reference values has improved tracking error.

7.1.5 Integral Action

Figure 6.2 shows that integral action is not necessary when considering torque generation. In fact, by penalizing the increment in the control signals the tracking error might increase as shown in Table 6.1.

7.2 Controller Performance

As mentioned earlier, and shown in Table 6.1, the formulated SLMPC controller with linearization about current operating point is unable to provide reasonable

results when testing with the WHTC. The controller manages to find solutions for parts of the test cycle, but the problems are introduced shortly after closed rack motoring where the controller is bypassed. In the problematic areas the MPC optimization problems become unfeasible. A solution to this is to increase the lower limit on the turbine rotational speed $x_{5,\min}$, but a too high limit of $x_{5,\min} > 3000$ rad/s is necessary to fully avoid the problem. This inevitably gives the controller much better but also unrealistic performance. The controller is therefore omitted from the controller performance data in Table 6.1. However, the test responses (see Figure 6.8, Figure 6.9, Figure 6.10 and Figure 6.11) look the most promising in terms of torque reference tracking when compared to test responses from the other examined controllers.

The LMPC controller – despite its simplicity – shows decent torque tracking in the test responses, but for some engine speeds the LMPC model will not be enough and the controller will not be able to deliver the desired torque, which is shown in Figure 6.7 and also reflected in Figure 6.17. Another issue with LMPC is that there seem to be small stationary errors in steady state for larger torque ranges as the linearized model about a single linearization point is unable to perfectly capture the model dynamics and therefore unable to perfectly track the state and control signal references in the larger torque ranges, for instance see Figure 6.4. For this reason, Table 6.1 also shows that the LMPC controller consumes less fuel than SLMPC: reference but also has significantly higher tracking error.

7.2.1 Smoke Limiter

Although the smoke limiter $\lambda > 1.2$ is included the optimization problems in the reference generation, see (4.1) and (4.2), there is no guarantee that there is no smoke generation during the transients. Short occurrences of $\lambda_O < 1$ can be noted for larger transients (see Figure 6.4, Figure 6.9 and Figure 6.13). Though, the smoke limiter works well in steady state as λ_O quickly increases again.

7.3 Future Work

Some ideas for future work are:

- Testing other types of outputs in the cost function of the MPC design to better compare and evaluate the results in Table 6.1. For instance MPC designs considering the output selections discussed in Section 2.4.1.
- Nonlinear MPC design.
- Investigate emission based MPC designs, such as including constraints on λ/λ_O and x_{egr} in the MPC design. Another approach is to extend the reference generator with requirements on EGR-fraction and study the engine in steady state.
- Even more focus on torque reference tracking, for instance by including requirements on the engine torque derivatives.

- Include limited peak pressure derivatives to avoid audible noise and potential engine damage.
- Include requirements on computational time and complexity in the MPC controller.

7.4 Conclusions

To conclude this thesis the questions proposed in Section 1.3 are answered.

- How can linearization based MPC be applied to control the fuel and air path of the diesel engine?

The fuel and air path of the diesel engine can be controlled using a reference generator that provides state and control signal references based on the desired torque and the engine speed from the drive cycle. The linearization based MPC controller ensures that fuel and air path adequately follow the references in steady state.

- How can performance requirements, such as torque response time, and requirements on safe operation, such as turbocharger overspeed protection, be introduced in the MPC controller?

Requirements on safe operation, such as turbocharger overspeed protection, are easily included as constraints in the MPC design. The performance of the MPC controller highly depends on the design parameters, for instance the weight matrices, sample rate and time horizon.

- How can diesel engine controller performances be measured and compared?

Diesel engine controller performances can be measured and compared using tracking errors, fuel consumption, particulate matter, nitric oxide emissions and much more.

- How do the considered linearization based MPC controllers compare in terms of performance?

The linearization based MPC yields decently accurate torque generation. Of the studied MPC controllers, the best performing design based on the evaluation with WHTC in Table 6.1 is the SLMPC with linearization about reference values (with preview and no integral action) as the most important measurement of performance in this thesis is low tracking error. In addition to lowest tracking error, the controller also has the best fuel consumption per mechanical work.

Appendix

A

MATLAB Model Representation

For some calculations it is necessary with a MATLAB model representation of the diesel engine. This chapter aims to validate the MATLAB model which is constructed based on the Simulink model described in [24].

A.1 MATLAB Model

The MATLAB model is expressed on the state space form:

$$\dot{x} = f(x, u, n_e)$$

where:

$$x = (p_{im} \quad p_{em} \quad X_{Oim} \quad X_{Oem} \quad \omega_t)^T, \qquad u = (u_\delta \quad u_{egr} \quad u_{vgt})^T$$

The MATLAB model uses one iteration of numerically calculated cylinder-out temperature as discussed in [24].

A.2 MATLAB Model Validation

The MATLAB model is validated using one of the two different run examples that are included in the downloadable model. The example studies a step from 30% to 25% in the VGT control signal, u_{vgt}. The MATLAB model states are calculated using MATLAB solver `ode15s` and the solution is compared with the Simulink simulation in Figure A.1.

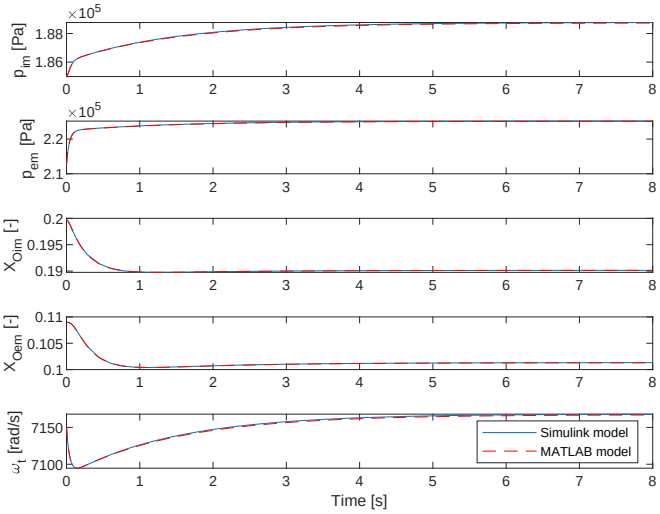

Figure A.1: *State comparison between MATLAB model and Simulink model*

Similarly the engine torque and oxygen-to-fuel ratio are compared in Figure A.2 for the same step.

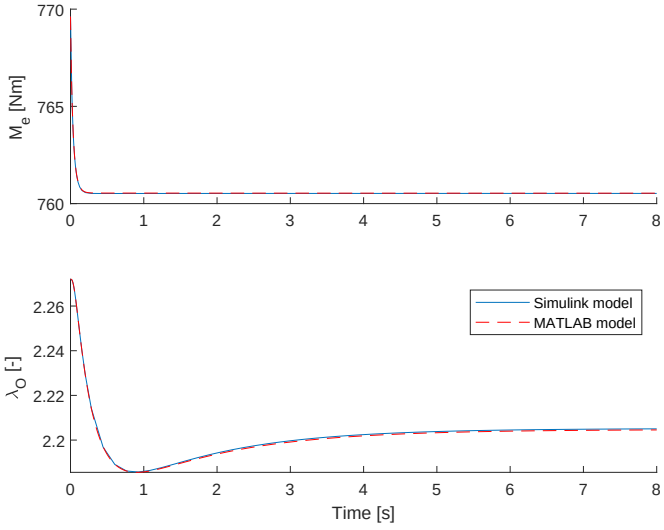

Figure A.2: *Engine torque and oxygen-to-fuel ratio comparison between MATLAB model and Simulink model*

A discretized version of integral absolute error, see (2.11), is utilized to further strengthen the validity of the MATLAB model. The error is then normalized with respect to the mean value of each Simulink measured state in Figure A.1. The resulting mean normalized absolute error is illustrated in Figure A.3.

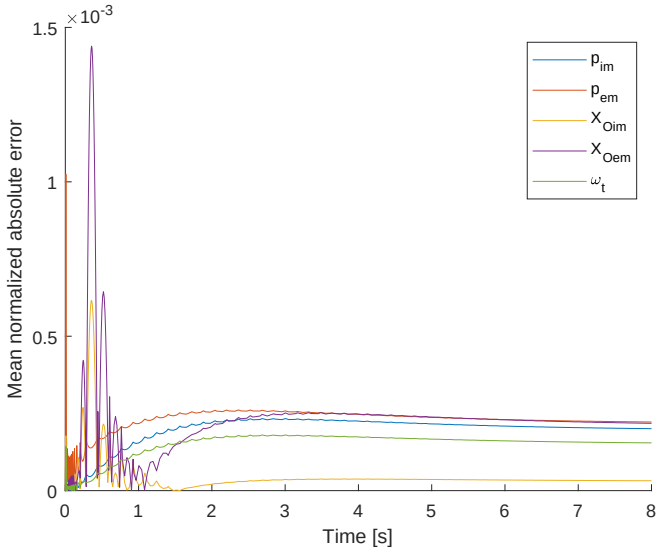

Figure A.3: *Absolute errors normalized with respect to state means for comparison in Figure A.1*

The errors can be reduced with an increased number of iterations on the numerically calculated cylinder-out temperature but at a cost of higher complexity. In conclusion, the MATLAB model is deemed accurate enough.

B

De-Normalization of WHTC

The WHTC test data is given in normalized engine speed and torque percentages. The data must be converted to engine specific values that are acquired during tests based on the engine-mapping curve. The de-normalization procedure follows the same structure as described by United Nations in [8].

B.1 Speed Profile

The engine speed profile is de-normalized according to (B.1).

$$\text{Actual speed} = 2.0327\frac{n_{\text{norm}}}{100}(0.45n_{\text{lo}} + 0.45n_{\text{pref}} + 0.1n_{\text{hi}} - n_{\text{idle}}) + n_{\text{idle}} \tag{B.1}$$

Where the speed variables are illustrated in [8] and summarized below.

n_{norm} is the normalized speed value

n_{idle} is the idle speed

n_{lo} is the lowest speed where the power is 55% of P_{max}

n_{pref} is the engine speed where the maximum torque integral is 51% of the integral from n_{idle} to n_{95}

n_{95} is the highest speed where the power is 95% of P_{max}

n_{hi} is the highest speed where the power is 70% of P_{max}

The speed values used in this thesis are based on the values from [2] due to lack of engine specific data, that is accurate representations of engine-mapping curve

and maximum power curve shown in Figure **??**. However, the engine examined in [2] is a hybrid electric truck which has engine speeds ranging from 500 rpm to 2400 rpm, whereas the model examined in this thesis ranges from 500 rpm to 2000 rpm, see (3.6). To account for the difference in engine speed ranges each test speed is rescaled after a translation to the origin, see (B.2).

$$n_{\text{rescale}} = (n - 500)\frac{2000 - 500}{2400 - 500} + 500 \tag{B.2}$$

The engine speed values are presented in Table B.1.

Table B.1: *Rescaled engine speeds used for de-normalization.*

Variable	**Value from** [2]	**Rescaled value using** (B.2)
n_{idle}	500 rpm	500 rpm
n_{lo}	815 rpm	749 rpm
n_{pref}	1418 rpm	1225 rpm
n_{95}	1966 rpm	1657 rpm
n_{hi}	2301 rpm	1922 rpm

However, the speed values in Table B.1 cannot guarantee an accurate representation of the actual speed values for the diesel engine examined in this thesis.

B.2 Torque Profile

The engine torque profile is de-normalized according to (B.3).

$$\text{Actual torque} = \frac{M_{\text{norm}}}{100} \cdot M_{\text{max/n}} \tag{B.3}$$

Where $M_{\text{max/n}}$ represents the maximum torque at the respective engine speed. As shown in Figure 2.1 the normalized torque values, M_{norm}, range from -10% to 100%. Negative values represent close rack motoring.

Due to lack of engine specific data the function $M_{\text{max/n}}$ is approximated by solving optimization problems on the form (B.4) for different engine speeds. The resulting engine-mapping curve is presented in Figure B.1 where the curve represents maximum torque at stationary points.

$$\begin{aligned} \max_{x,u} \quad & M_e \\ \text{subject to} \quad & \dot{x} = f(x, u, n_e) = 0 \\ & \lambda(x, u) \geq 1.2 \\ & x_{\min} \leq x \leq x_{\max} \\ & u_{\min} \leq u \leq u_{\max} \end{aligned} \tag{B.4}$$

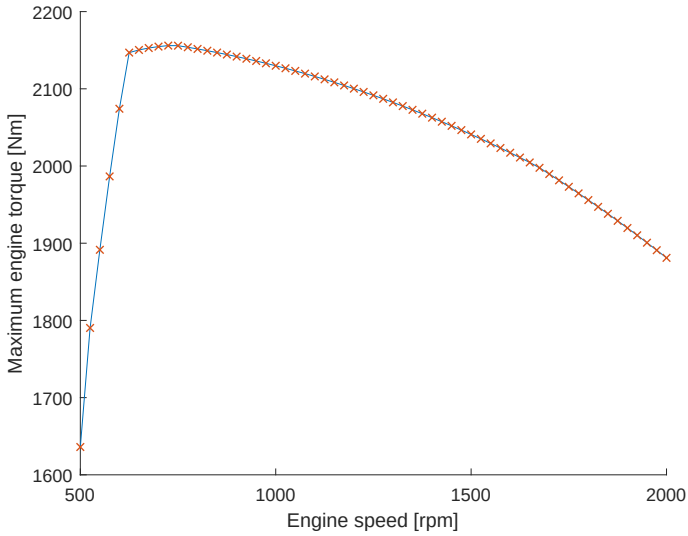

Figure B.1: *Maximum torque curve, $M_{\max/n}$, for stationary points*

B.3 De-Normalized Test Data

The normalized test data in Figure 2.1 is then de-normalized using (B.1) and (B.3), see Figure B.2.

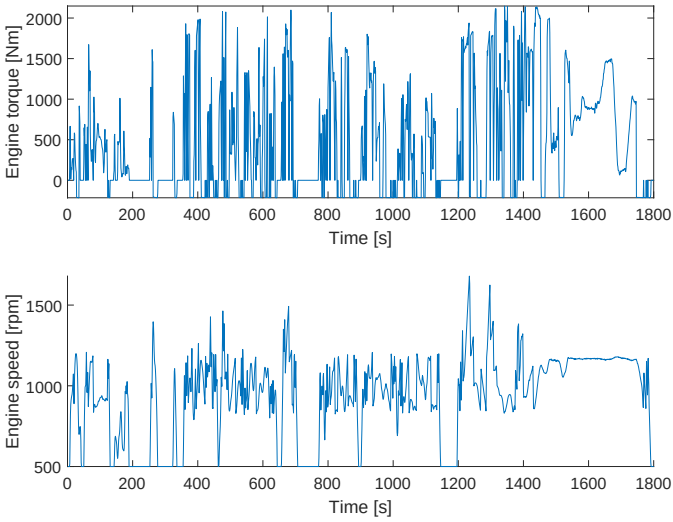

Figure B.2: *De-normalized test data.*

C

Lookup Table Data

C.1 State Reference Values

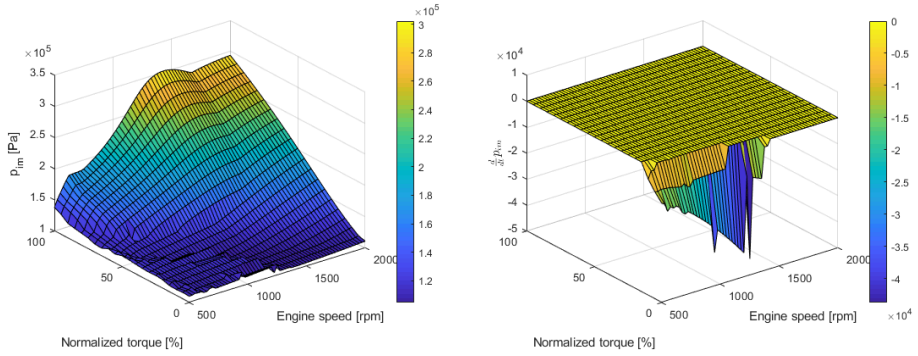

Figure C.1: *Lookup table data for intake manifold pressure, p_{im}, and its derivative, $\frac{d}{dt}p_{\mathrm{im}}$*

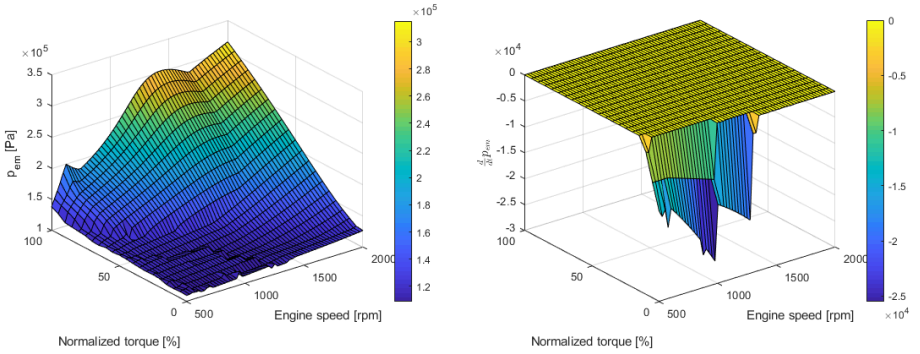

Figure C.2: *Lookup table data for exhaust manifold pressure, p_{em}, and its derivative, $\frac{d}{dt}p_{\mathrm{em}}$*

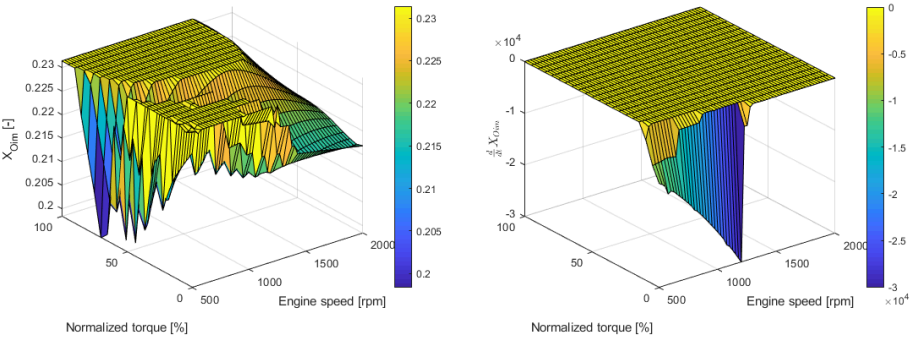

Figure C.3: *Lookup table data for intake manifold oxygen mass fraction, X_{Oim}, and its derivative, $\frac{d}{dt}X_{\mathrm{Oim}}$*

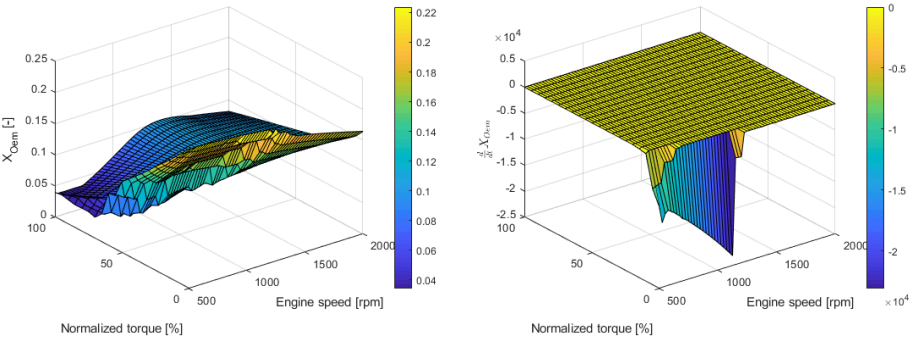

Figure C.4: *Lookup table data for exhaust manifold oxygen mass fraction, X_{Oem}, and its derivative, $\frac{d}{dt}X_{\mathrm{Oem}}$*

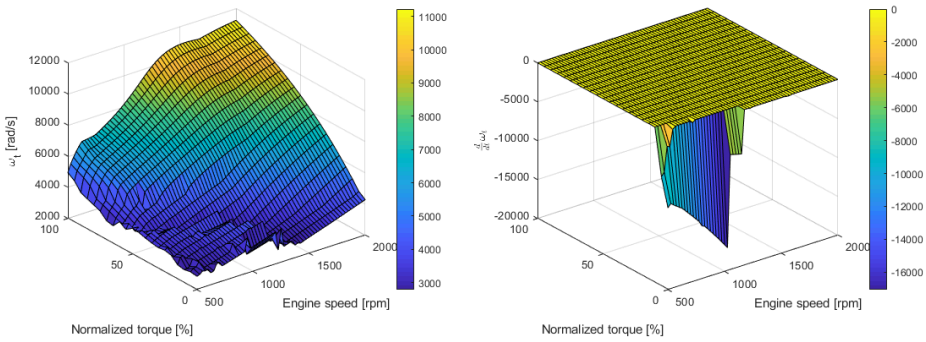

Figure C.5: *Lookup table data for turbine speed, ω_t, and its derivative, $\frac{d}{dt}\omega_t$*

C.2 Control Signal Reference Values

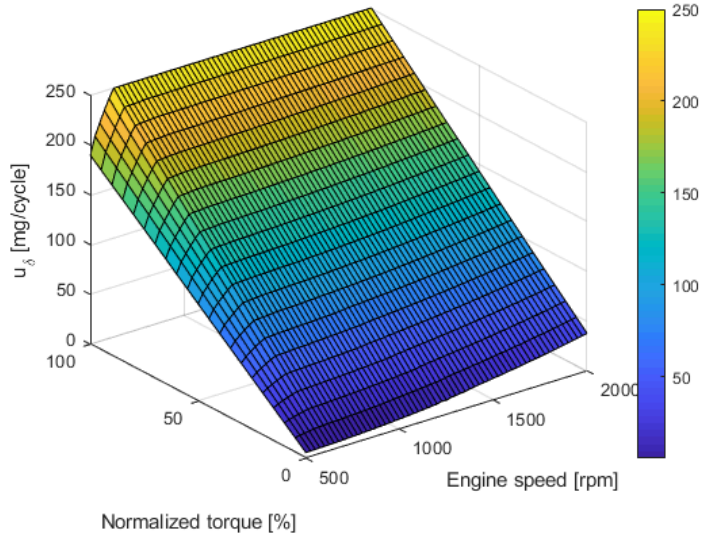

Figure C.6: *Lookup table data for injected fuel per cylinder, u_δ*

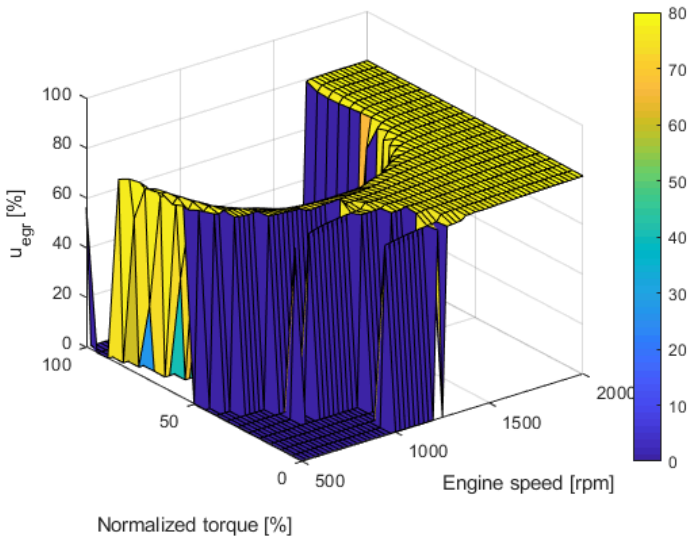

Figure C.7: *Lookup table data for EGR control signal,* u_{egr}

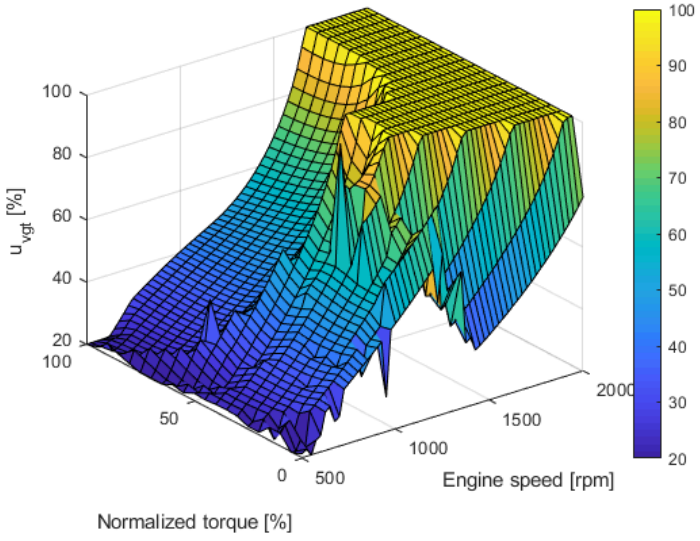

Figure C.8: *Lookup table data for VGT control signal,* u_{vgt}

D

Weight Matrices

Weight matrices to LMPC and SLMPC controllers where the minimum and maximum values are presented in (3.4), (3.5) and (3.6).

$$Q_1 = \begin{bmatrix} \frac{10}{(\frac{x_{1,\min}+x_{1,\max}}{2})^2} & 0 & 0 & 0 & 0 \\ 0 & \frac{10}{(\frac{x_{2,\min}+x_{2,\max}}{2})^2} & 0 & 0 & 0 \\ 0 & 0 & \frac{1}{(\frac{x_{3,\min}+x_{3,\max}}{2})^2} & 0 & 0 \\ 0 & 0 & 0 & \frac{1}{(\frac{x_{4,\min}+x_{4,\max}}{2})^2} & 0 \\ 0 & 0 & 0 & 0 & \frac{10}{(\frac{x_{5,\min}+x_{5,\max}}{2})^2} \end{bmatrix}$$

$$Q_2 = \begin{bmatrix} \frac{5}{(\frac{u_{1,\min}+u_{1,\max}}{2})^2} & 0 & 0 \\ 0 & \frac{0.05}{(\frac{u_{2,\min}+u_{2,\max}}{2})^2} & 0 \\ 0 & 0 & \frac{0.05}{(\frac{u_{3,\min}+u_{3,\max}}{2})^2} \end{bmatrix}$$

$$Q_3 = \begin{bmatrix} \frac{0.05}{(\frac{u_{1,\min}+u_{1,\max}}{2})^2} & 0 & 0 \\ 0 & \frac{0.05}{(\frac{u_{2,\min}+u_{2,\max}}{2})^2} & 0 \\ 0 & 0 & \frac{0.05}{(\frac{u_{3,\min}+u_{3,\max}}{2})^2} \end{bmatrix}$$

$$Q_4 = Q_1$$

Bibliography

[1] Daniel Alberer and Luigi del Re. On-line abatement of transient NOx and PM diesel engine emissions by oxygen based optimal control. In *SAE 2010 Powertrains Fuels Lubricants Meeting*. SAE International, oct 2010. doi: https://doi.org/10.4271/2010-01-2201. URL https://doi.org/10.4271/2010-01-2201.

[2] Fredrik Andersson and Hampus Andersson. Numerical optimal control of hybrid electric trucks: Exhaust temperature, NOx emission and fuel consumption. Master's thesis, Linköping University, 2018.

[3] Joel A. E. Andersson, Joris Gillis, Greg Horn, James B. Rawlings, and Moritz Diehl. CasADi – A software framework for nonlinear optimization and optimal control. *Mathematical Programming Computation*, In Press, 2018.

[4] Volkan Aran. Flexible and robust control of heavy duty diesel engine airpath using data driven disturbance observers and GPR models, July 2019. URL http://research.sabanciuniv.edu/39260/.

[5] Bo Bernhardsson and Karl Johan Åström. Model predictive control (MPC), 2016. URL http://www.control.lth.se/fileadmin/control/Education/DoctorateProgram/ControlSystemsSynthesis/2016/MPC.pdf. [Online; accessed 2021-02-09].

[6] Martin Enqvist, Torkel Glad, Svante Gunnarsson, Peter Lindskog, Lennart Ljung, Johan Löfberg, Tomas McKelvey, Anders Stenman, and Jan-Erik Strömberg. *Industriell reglerteknik: Kurskompendium*. Reglerteknik, Institutionen för systemteknik, Linköpings universitet, 2014.

[7] Lars Eriksson. Matlab/simulink model for a turbocharged diesel engine with EGR and VGT. https://www.vehicular.isy.liu.se/Software/TCDI_EGR_VGT/, 2013. [Online; accessed 2020-10-12].

[8] UN. ECE. World Forum for Harmonization of Vehicle Regulations. Working Party on Pollution and Energy (52nd sess. : 2006 : Geneva). Proposal for a draft global technical regulation (GTR): Test procedure for compression-ignition (C.I) engines and positive-ignition (P.I) engines fuelled with natu-

ral gas (NG) or liquefied petroleum gas (LPG) with regard to the emission of pollutants : world-wide harmonized heavy-duty certification (WHDC) procedure. Jul 2006. URL http://digitallibrary.un.org/record/579589. Adopted by the Working Party on Pollution and Energy at its 52nd session; based on document ECE/TRANS/WP.29/GRPE/2006/17.

[9] Esteban R. Gelso and Johan Dahl. Diesel engine control with exhaust aftertreatment constraints. *IFAC-PapersOnLine*, 50(1):8921 – 8926, 2017. ISSN 2405-8963. doi: https://doi.org/10.1016/j.ifacol.2017.08.1293. URL http://www.sciencedirect.com/science/article/pii/S240589631731813X. 20th IFAC World Congress.

[10] Torkel Glad and Lennart Ljung. *Reglerteori: Flervariabla och olinjära metoder*. Studentlitteratur AB, 2017. ISBN 978-91-44-03003-6.

[11] Lino Guzzella and Alois Amstutz. Control of diesel engines. *IEEE Control Systems Magazine*, 18(5):53–71, 1998. doi: 10.1109/37.722253.

[12] Mikael Johansson. EL2520 Control Theory and Practice. Lecture 13: Model predictive control. URL https://www.kth.se/social/upload/5194b526f276547b030b4bcb/lec13_mpc2_1up.pdf. [Online; accessed 2021-02-29].

[13] Maria Karlsson, Kent Ekholm, Petter Strandh, Rolf Johansson, and Per Tunestål. Multiple-input multiple-output model predictive control of a diesel engine. *IFAC Proceedings Volumes*, 43(7):131 – 136, 2010. ISSN 1474-6670. doi: https://doi.org/10.3182/20100712-3-DE-2013.00003. URL http://www.sciencedirect.com/science/article/pii/S147466701536818X. 6th IFAC Symposium on Advances in Automotive Control.

[14] Mikhail Konnik and Jose Dona. Hot-start efficiency of quadratic programming algorithms for fast model predictive control: A comparison via an adaptive optics case study. 11 2014. doi: 10.1109/AUCC.2014.7358641.

[15] Thomas E. Marlin. *Process Control: Designing Processes and Control Systems for Dynamic Performance*, page 219. McGraw-Hill, 2 edition, 1995.

[16] Martin Mönnigmann. What are the advantages of model predictive control over optimal control?, January 2016.

[17] Jonas Olsson and Markus Welander. Optimal control of diesel engine with VGT and EGR. Master's thesis, Linköping University, June 2006.

[18] Peter Ortner, Peter Langthaler, José Vicente Garcia Ortiz, and L. del Re. MPC for a diesel engine air path using an explicit approach for constraint systems. In *2006 IEEE Conference on Computer Aided Control System Design, 2006 IEEE International Conference on Control Applications, 2006 IEEE International Symposium on Intelligent Control*, pages 2760–2765, 2006. doi: 10.1109/CACSD-CCA-ISIC.2006.4777060.

[19] James B. Rawlings, David Q. Mayne, and Moritz M. Diehl. *Model Predictive Control: Theory, Computation, and Design*. Nob Hill Publishing, LLC, 2 edition, 2019.

[20] Joachim Rückert, Felix Richert, Axel Schloer, Dirk Abel, Olaf Herrmann, Stefan Pischinger, and Andreas Pfeifer. A model based predictive attempt to control boost pressure and EGR-rate in a heavy duty diesel engine. *IFAC Proceedings Volumes*, 37(22):111 – 117, 2004. ISSN 1474-6670. doi: https://doi.org/10.1016/S1474-6670(17)30330-0. URL http://www.sciencedirect.com/science/article/pii/S1474667017303300. IFAC Symposium on Advances in Automotive Control 2004, Salerno, Italy, 19-23 April 2004.

[21] Gokul S. Sankar, Rohan C. Shekhar, Chris Manzie, Takeshi Sano, and Hayato Nakada. Fast calibration of a robust model predictive controller for diesel engine airpath. *IEEE Transactions on Control Systems Technology*, 28(4): 1505–1519, 2020.

[22] Yusuf A. Sha'aban, Barry Lennox, and David Laurí. PID versus MPC performance for SISO dead-time dominant processes*. *IFAC Proceedings Volumes*, 46(32):241 – 246, 2013. ISSN 1474-6670. doi: https://doi.org/10.3182/20131218-3-IN-2045.00054. URL http://www.sciencedirect.com/science/article/pii/S1474667015382641. 10th IFAC International Symposium on Dynamics and Control of Process Systems.

[23] United Nations. UN GTR No. 4 - Test procedure for compression-ignition (C.I.) engines and positive-ignition (P.I.) engines fuelled with natural gas (NG) or liquefied petroleum gas (LPG) with regard to the emission of pollutants. https://www.unece.org/trans/main/wp29/wp29wgs/wp29gen/wp29glob_registry.html, 2004. URL https://www.unece.org/trans/main/wp29/wp29wgs/wp29gen/wp29glob_registry.html.

[24] Johan Wahlström and Lars Eriksson. Modelling diesel engines with a variable-geometry turbocharger and exhaust gas recirculation by optimization of model parameters for capturing non-linear system dynamics. *Proceedings of the Institution of Mechanical Engineers, Part D: Journal of Automobile Engineering*, 225(7):960–986, 2011. doi: 10.1177/0954407011398177. URL https://doi.org/10.1177/0954407011398177.

[25] Johan Wahlström and Lars Eriksson. Output selection and its implications for MPC of EGR and VGT in diesel engines. *IEEE Transactions on Control Systems Technology*, 21(3):932–940, May 2013.

[26] Altay Zhakatayev, Bexultan Rakhim, Olzhas Adiyatov, Almaskhan Baimyshev, and Huseyin A. Varol. Successive linearization based model predictive control of variable stiffness actuated robots. In *2017 IEEE International*

Conference on Advanced Intelligent Mechatronics (AIM), pages 1774–1779, 2017. doi: 10.1109/AIM.2017.8014275.